MECHANISM OF SEMAPHORIN-PLEXIN SIGNALING IN SYNAPTIC PATTERN FORMATION IN *CAENORHABDITIS ELEGANS*

by

Xi Chen

B.Sc., China Pharmaceutical University, 2009

A THESIS SUBMITTED IN PARTIAL FULFILLMENT OF
THE REQUIREMENTS FOR THE DEGREE OF

MASTER OF SCIENCE

in

THE FACULTY OF GRADUATE AND POSTDOCTORAL STUDIES
(Zoology)

THE UNIVERSITY OF BRITISH COLUMBIA
(Vancouver)

October 2017

Abstract

Fine motor coordination depends on the precise synaptic connection between individual motor neurons and muscles. Recent studies have revealed the roles of extracellular signals such as Wnt, Netrin, and Semaphorin in synapse specificity. Little is known about their intracellular mechanisms in synapse patterning.

In *C. elegans*, DA class motor neurons form en passant synapses along their axon on the dorsal nerve cord. Each DA neuron innervates a unique and tiled segment of muscle field by restricting its synapse to a distinct subaxonal domain - a phenomenon we term synaptic tiling. SEMAs/Semaphorins and their receptor PLX-1/Plexin were previously shown to be critical for the tiled synaptic innervation pattern between two neighboring neurons DA8 and DA9. Recently, structural and biochemical studies have predicted that mammalian Plexin acts as a GTPase activating protein (GAP) for Rap small GTPases.

In this study, among three *rap* genes in the *C. elegans* genome, *rap-2* is found to be required for synaptic tiling and functions through cycling between GTP- and GDP-bound forms. The genetic study has illustrated that *rap-2* acts downstream of *plx-1* to regulate synaptic tiling, supporting that PLX-1 acts as a RapGAP to regulate the spatial activity of RAP-2. MIG-15 is identified as an effector of RAP-2 in synaptic tiling. *mig-15* mutants display severe synaptic tiling defects due to the increased synapse number of DA8 and DA9.

MIG-15 overexpression experiments demonstrated that MIG-15 controls both the length of synaptic domain and the number of synapses, while Plexin and RAP-2 define the length of the synaptic domain. PLX-1 overexpression experiments indicated that PLX-1 specifies synapse distribution via RAP-2 small GTPase and MIG-15 kinase. Overall, this study identified two novel components of Plexin signaling in the spatial regulation of synaptic pattern formation.

Lay Summary

Our nervous system forms a complex network, which is composed of an estimated 100 billion neurons coordinating with their targets. A neuron innervates by forming the synapse with its precise target. Previous work from our lab has shown that the loss of the *Plexin* gene in a motor neuron results in the disruption of innervation. However, the underlying mechanism causing this disorganization is unknown. My study has provided the first evidence that two genes, *Rap2* and *TNIK,* cooperate with *Plexin* activity to regulate the formation and distribution of synapses along the same motor neuron. Because it has been reported that *Rap-2* and *TNIK* are involved in immune responses, mental disorders, and cancers, my study provides possible insights into identifying new therapeutic approaches related to these physiological and pathological processes.

Preface

All the works described in this thesis are completed by me under the supervision of Dr. Kota Mizumoto in Life Sciences Institute, at the University of British Columbia. Dr. Kota Mizumoto and I designed all the experiments together, and I collected and analyzed all the data under the supervision of Dr. Kota Mizumoto. I prepared the initial and final drafts of this thesis, which was edited and approved by my supervisor, Dr. Donald Moerman, and Dr. Linda Matsuuchi. A manuscript based on Chapter 2 to Chapter 5 is currently in preparation for a publication.

Table of Contents

Abstract ..... **ii**

Lay Summary ..... **iv**

Preface ..... **v**

Table of Contents ..... **vi**

List of Figures ..... **ix**

List of Abbreviations ..... **xi**

Acknowledgements ..... **xiii**

Chapter 1: Introductions **1**

1.1 Synaptic pattern formation 1

1.2 Synaptic tiling of *C. elegans* 2

1.3 The marker system for visualizing and distinguishing DA synapses 4

1.4 Semaphorin-Plexin signaling is required for synaptic tiling 5

1.5 Semaphorin-Plexin signaling 6

1.6 PLX-1 requires its RapGAP domain to regulate synaptic tiling 8

1.7 Rap small GTPases 9

1.7.1 Cycling of small GTPase 9

1.7.2 The function of Rap small GTPases 9

1.8 *mig-15*/*TNIK* kinase gene 11

1.8.1 Structural analysis of MIG-15 11

1.8.2 Role of TNIK in actin cytoskeleton dynamics 12

1.9 Aims of this thesis 13

Chapter 2: Materials and Methods **14**

2.1 Strains and genotype validation 14

2.1.1 Strains and worm culture 14

2.1.2 DNA extraction and polymerase chain reaction 14

2.2 Plasmids and construction 16

2.3 CRISPR/Cas9 genome editing 18

2.4 Quantitative PCR 19

2.5 Confocal Microscopy 20

2.6 Statistics 20

2.7 Image processing 20

Chapter 3: The Role of the *rap-2* Gene in Synaptic Tiling 21

3.1 *rap-2* is responsible for synaptic tiling 21

3.1.1 Constitutively GTP-bound RAP-1 and GTP-bound RAP-2 both induce synaptic tiling defects 21

3.1.2 *rap-2* mutants show synaptic tiling defects 23

3.1.3 Synaptic tiling defect of *rap-2* mutant is caused by the extension of DA8 and DA9 synaptic domains 26

3.2 *rap-2* genetically acts in the same pathway with *plx-1* 27

3.3 *rap-2* acts cell autonomously in DA neurons 28

3.4 The cycling of RAP-2 is required for synaptic tiling 31

3.4.1 Generating constitutively GTP-bound *rap-2* and GDP-bound *rap-2* mutants 31

3.4.2 Both GTP-RAP-2 and GDP-RAP-2 are required to regulate synaptic tiling 32

3.5 Detecting GTP-RAP-2 and GDP-RAP-2 at the subcellular level 33

3.6 Discussion 35

3.7 Conclusions 37

Chapter 4: The Role of the *mig-15* Gene in Synaptic Tiling 38

4.1 *mig-15* is required for synaptic tiling 38

4.2 *mig-15* mutants show DA9 axon defect 40

4.3 *mig-15* genetically acts in the same pathway with *rap-2* and *plx-1* 42

4.4 *mig-15* acts cell autonomously in DA neurons 44

4.5 The localization of MIG-15 in DA9 46

4.6 *mig-15* functions as a negative regulator of DA9 synapse formation 48

4.7 PLX-1/RAP-2 signaling coordinates DA8/DA9 synaptic border 50

4.8 *mig-15* might regulate synapse number via F-actin 51

4.9 Discussion 52

4.10 Conclusions 55

Chapter 5: Relationship Study of *plx-1*, *rap-2* and *mig-15* 56

5.1 *mig-15* requires *plx-1* and *rap-2* to specify DA9 synaptic domain 56

5.2 *plx-1* regulates *mig-15* via *rap-2* to specify DA9 synaptic domain 58

5.3 Discussion 60

5.4 Conclusions 63

Chapter 6: The Model of DA8/DA9 Synaptic Tiling and Future Directions .. 64

6.1 The model of the DA8/DA9 synaptic tiling 64

6.2 Future directions 67

Bibliography 69

List of Figures

Figure 1.1 Schematic of synaptic tiling of DA class motor neurons (DA6-DA9) (White et al., 1976). 3

Figure 1.2 DA8 and DA9 synaptic tiling of wild-type *C. elegans.* 4

Figure 1.3 *plx-1* is required to maintain DA8/DA9 synaptic tiling (Mizumoto, 2013). 6

Figure 3.1 RAP-1 G12V and RAP-2 G12V both induced synaptic tiling defects. . 23

Figure 3.2 The *rap-2* gene is required for DA8/DA9 synaptic tiling and expressed in DA neurons. 26

Figure 3.3 DA8 and DA9 synaptic domains are both extended in *rap-2* mutants. 27

Figure 3.4 *plx-1* and *rap-2* genetically act in the same pathway. 28

Figure 3.5 *rap-2* acts cell autonomously in DAs. 31

Figure 3.6 The sequence and unchanged expression levels of five *rap-2* mutants generated by CRISPR/Cas9. 32

Figure 3.7 Constitutively GTP- and GDP-bound *rap-2* mutants show synaptic tiling defects and do not enhance *plx-1*. 33

Figure 3.8 Localization of GTP-RAP-2 and GDP-RAP-2. 34

Figure 4.1 *mig-15* is required for synaptic tiling. 40

Figure 4.2 DA9 axon defects of *mig-15* mutants. 41

Figure 4.3 *mig-15* genetically acts in the same pathway with *plx-1* and *rap-2.* 44

Figure 4.4 *mig-15* acts in DA9 in a cell-autonomous manner. 46

Figure 4.5 Localization of MIG-15. 47

Figure 4.6 *mig-15* is a negative regulator of synapse formation. 49

Figure 4.7 PLX-1 signaling adjusts DA8/DA9 synaptic boundary 51

Figure 4.8 *mig-15* might regulate synapse number via F-actin. 52

Figure 5.1 *mig-15* requires *rap-2* to specify DA9 synaptic domains..... 58

Figure 5.2 *plx-1* regulates *mig-15* via *rap-2* to specify DA9 synaptic domains..... 60

Figure 6.1 The Model of the DA8/DA9 synaptic tiling. 67

List of Abbreviations

BDM	2, 3-butanedionemonoxime
cDNA	complementary DNA
C. elegans	*Caenorhabditis elegans*
CNH	Citron Homology
DA	Dorsal A class
Ex	Extrachromosomal
F-actin	Filamentous actin
GAP	GTPase Activating Protein
GCKH	Germinal Center Kinase Homolog
GDP	Guanosine diphosphate
GEF	GTP Exchange Factor
GFP	Green Fluorescent Protein
GTP	Guanosine triphosphate
JNK	c-Jun N-terminal kinase
L2	Larvae 2
L3	Larvae 3
L4	Larvae 4
MAPK4	Mitogen-Activated Protein Kinase 4
mCherry	mCherry fluorescent protein
MINK	Mishapen/NIKs-related Kinase
myr	myristolated

OE	Over Expression
PCR	Polymerase Chain Reaction
qPCR	quantitative Polymerase Chain Reaction
RT-PCR	Reverse Transcription-Polymerase Chain Reaction
sgRNA	small guide RNA
SEMA	Semaphorin
Ste20	Sterile 20 protein
TNIK	Traf2- and Nck-interacting kinase
Ut-CH	Utrophin Calponin Homology domain

Acknowledgements

First and foremost, I am grateful to have the full support from my supervisor Dr. Kota Mizumoto who offered me the opportunity to pursue this study and guided me through the whole project.

I would like to acknowledge my supervisory committee members, Dr. Donald Moerman and Dr. Linda Matsuuchi, for their support and suggestions during my master study. I would also like to thank them for reading through and editing this thesis.

Also, I would like to express my thanks to the members of Mizumoto lab. The special thank-you is for the members of the Moerman lab, who provided lots of technical supports to this study.

Chapter 1: Introductions

1.1 Synaptic pattern formation

Our nervous system consists of approximately 100 billion neurons and functions by properly innervating its targets. One neuron, surrounded by a complex environment, forms neuronal circuits step by step: cell fate determination, migration, dendrite and axon protrusion, growth and guidance and synapse formation. During these processes, the neuron eventually specifies the connectivity with its target.

In the mammalian olfactory system, the axon of a sensory neuron in the epithelial cell layer, which solely expresses a specific odor receptor, only connects with a single glomerulus in the olfactory bulb. By this site-to-site connectivity, mammals can potentially distinguish 400,000 different compounds (Buck, 1996; Mombaerts et al., 1996; Mori and Yoshihara, 1995; Mori et al., 2006; Ressler et al., 1994; Stewart et al., 1979; Vassar et al., 1994). In the visual system of *Drosophila*, a compound eye is composed of 800 simple eyes, each containing 8 cells that precisely connect with a certain group of lamina or medulla neurons (Braitenberg, 1967; Clandinin and Zipursky, 2002; Kirshfeld, 1967; M Bate, A Martinez-Arias (Eds.); Trujillo-Cenóz, 1965; Trujillo-Cenoz and Melamed, 1966; Vigier, P, 1909), so that the stimuli received from different directions could be accurately integrated by the visual system. For decades, neuroscientists have tried to determine how a neuron precisely navigates to form neural circuits. Research work over the past 20 years has elucidated that precise innervation is mediated by cell-cell molecular interactions, for

instance, *C. elegans* immunoglobulin proteins SYG-1/Neph1 and SYG-1/Nephrin, and spatial gradients of molecular cues, such as Wnts (Ango et al., 2004; Klassen and Shen, 2007; Mizumoto and Shen, 2013a; Shen and Bargmann, 2003). Recently, some axon guidance cues such as Netrin/DCC and Semaphorin/Plexin, were found to regulate synaptic pattern formation, however, little is known about the intracellular mechanisms of these signals (Ding et al., 2012; Mizumoto and Shen, 2013b; Pecho-Vrieseling et al., 2009; Timofeev et al., 2012). How do these signals regulate intracellular activities to form precise synapse? This question has led researchers to explore the intracellular components of the above-mentioned signaling pathways.

1.2 Synaptic tiling of *C. elegans*

The nematode *Caenorhabditis elegans (C. elegans)* is a model organism used to study the mechanism of synaptic pattern formation. This model system has the following advantages: 1) nematode genes show high identity and similarity to human genes; 2) the nervous system of hermaphrodites is composed of 302 completely mapped neurons and their connectomes; and 3) the transparency enables people to perform in vivo research at not only the cellular but also the subcellular level as well.

In the 1970s, John White completed the connectomics of *C. elegans* by tracing >8000 serial ultrathin sections from this 1mm long creature. By using electron microscopy, White and colleagues interpreted the elaborate synaptic patterns of *C. elegans*. Taking the cholinergic dorsal A (DA) class motor neurons as an example: the cell bodies and dendrites of DA neurons reside on the ventral side

while projecting their axons to the dorsal nerve cord, where the axon of each neuron innervates a certain segment of dorsal muscle in a non-overlapped but “tiled” manner (Figure 1.1). Not only DA, but other classes of motor neurons such as ventral A, ventral B, and dorsal B also innervate their targets in this manner (White et al., 1976). This “tiled” feature of synaptic patterning is termed as “synaptic tiling” (Mizumoto and Shen, 2013b). This highly organized synaptic patterning allows us to screen for the mutants that exhibit anomalies in synaptic tiling and to identify the genes that are responsible for the regulation of synaptic tiling.

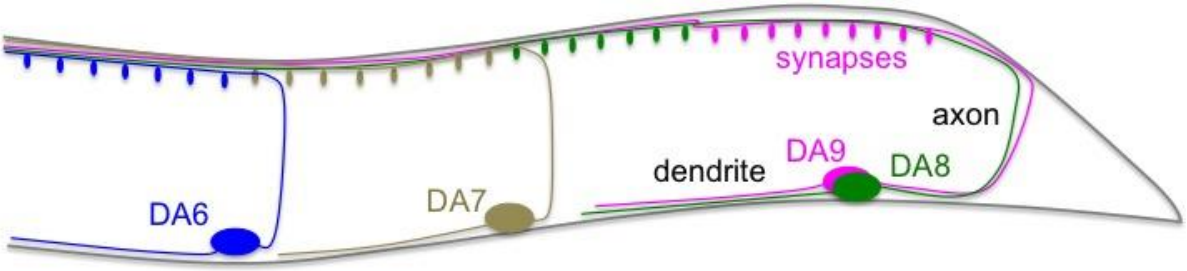

Figure 1.1 Schematic of synaptic tiling of DA class motor neurons (DA6-DA9) (White et al., 1976).

Cell bodies are shown as big circles with different colors (blue for DA6, ochre for DA7, green for DA8 and magenta for DA9) and smaller ovals of the corresponding color represent multiple synapses of each DA neuron. DA8/DA9 dendrites and axons are labeled and color-coded.

1.3 The marker system for visualizing and distinguishing DA synapses

In order to explore the molecular mechanism of synaptic tiling of DA neurons, Mizumoto developed a marker system to visualize and distinguish the synapses of DA8 and DA9 neurons (Mizumoto and Shen, 2013b). Firstly, the synapses of all DA neurons are labeled by green fluorescent protein (GFP) fused with the small GTPase RAB-3, which is required by synaptic vesicle recruitment (Nonet et al., 1997). Second, the synapses of DA9 are distinguishably labeled by mCherry fluorescent protein (mCherry) fused with RAB-3. After being visualized, the synapses of DA8 and DA9 can be detected by fluorescent microscopy, and a clear boundary between DA8 and DA9 synaptic domains is shown in wild-type background animals as illustrated in Figure 1.2.

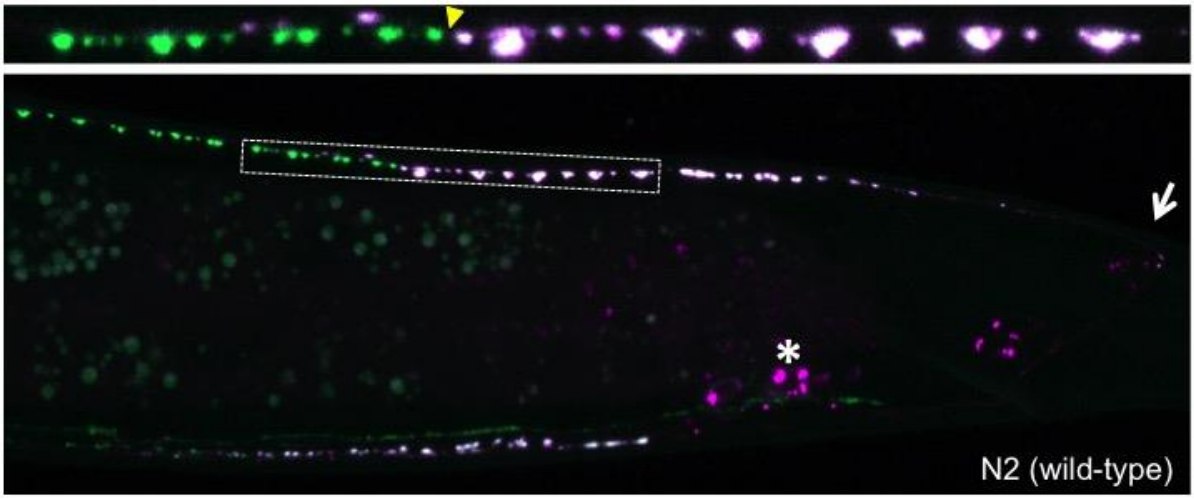

Figure 1.2 DA8 and DA9 synaptic tiling of wild-type *C. elegans.*

Synapses of all DA neurons are labeled with GFP::RAB-3, synapses of DA9 are labeled with mCherry::RAB-3. Arrow indicates the DA9 axon, the asterisk indicates cell body of DA9, the framed region is straightened and magnified to show the boundary between DA8 and DA9 synaptic domains, which is indicated by the yellow arrowhead.

1.4 Semaphorin-Plexin signaling is required for synaptic tiling

Previous research from our group found that the mutants of the *plx-1* gene (homolog of human Plexin) show synaptic tiling defect (Figure 1.3 A). In *plx-1* mutants, the DA8 synaptic domain extends posteriorly and the DA9 synaptic domain extends anteriorly and, as a consequence, the synapses of DA8 and DA9 neurons intermingled with each other. Further tests proved that this phenotype is caused by the absence of *plx-1* in DA9 neuron, which means that the *plx-1* gene acts cell autonomously to maintain the clear synaptic boundary between DA8 and DA9. GFP tagged PLX-1 was detected to be consistently enriched at the anterior border of the DA9 synaptic domain (Figure 1.3 B). Based on these observations, Mizumoto proposed that PLX-1 specifies the synaptic border of the DA9 neuron by localizing at the anterior synapse free domain (Mizumoto and Shen, 2013b).

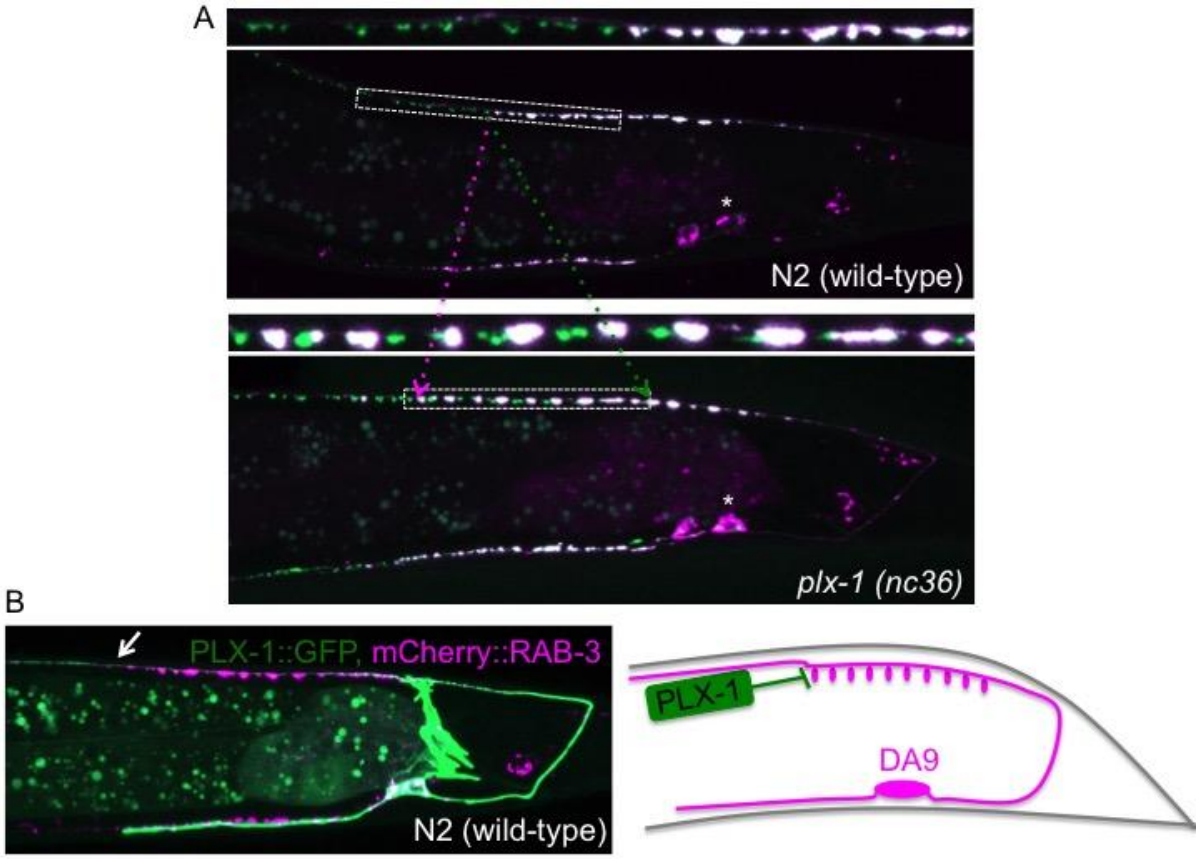

Figure 1.3 *plx-1* is required to maintain DA8/DA9 synaptic tiling (Mizumoto, 2013).

(A) Synaptic tiling defect of *plx-1* mutants, DA8 and DA9 synaptic domains extend into each other, magenta arrow denotes the most anterior DA9 synapse and green arrow denotes the most posterior DA8 synapse. (B) PLX-1::GFP is enriched at the DA9 synaptic border (indicated by the white arrow).

1.5 Semaphorin-Plexin signaling

Plexins are a class of transmembrane proteins, which show high identity and similarity across species (Nakao et al., 1999; Tamagnone et al., 1999). Plexins function as receptors of Semaphorins that are composed of secreted, membrane-anchored and transmembrane subtype family members (Kolodkin et al., 1993;

Winberg et al., 1998). Semaphorin-Plexin functions as a repellent signal to regulate a number of physiological and pathogenic activities. After first being identified as an axonal guidance cue (Kolodkin et al., 1993), it was also reported to be involved in the immune response (Kumanogoh et al., 2005), bone homeostasis (Hayashi et al., 2012; Negishi-Koga et al., 2011), cardiovascular development (Toyofuku and Kikutani, 2007; Toyofuku et al., 2008) and tumor progression (Luchino et al., 2013).

Regarding synaptogenesis, it has been shown that the specific recognition of Sema3e-Plxnd1 generates a repellent signal to specify the connectivity between proprioceptive sensory neurons (which express Plxnd1) and a certain group of triceps motor neurons (which do not express Sema3e) hence to form the monosynaptic connections (Pecho-Vrieseling et al., 2009). Semaphorin-Plexin signaling predominantly results in changes to the cytoskeletal and adhesive machinery that regulate cellular morphology. This process is associated with small GTPases activities (Alto and Terman, 2017).

Because *sema* and *plx-1* genes are required to maintain synaptic tiling (Mizumoto and Shen, 2013b), I hypothesized that the recognition between SEMAs and PlX-1 can trigger a repellent intracellular cascade to negatively regulate synapse formation at the DA9 synaptic border, and the underlying mechanism is through regulating the activities of small GTPases by the intracellular portion of PLX-1.

1.6 PLX-1 requires its RapGAP domain to regulate synaptic tiling

The cytoplasmic GAP domain of Plexin inactivates the small GTPase R-Ras: the activation of Plexins stimulated by Semaphorins repulses axon outgrowth through inhibiting R-Ras (Oinuma et al., 2004; Rohm et al., 2000). Mizumoto showed that *let-60*, a *C. elegans* Ras gene is involved in Plexin signaling to regulate synaptic tiling (Mizumoto and Shen, 2013b).

More recently, a systematic analysis of most Plexin family members from mouse has elaborated that Plexins contain an intracellular RapGAP domain, which functions as an activating protein of Rap small GTPases, a class of subfamily members of Ras (Pascoe et al., 2015a; Wang et al., 2013). In *plx-1* knockout mutants, when the intact PLX-1 expression was restored in DA9 neurons, the synaptic tiling defect was rescued. In contrast, expression of the PLX-1 protein with no cytoplasmic portion failed to rescue the overlap between DA8 and DA9 synaptic domains (Mizumoto and Shen, 2013b). The implication from these results is that PLX-1 requires its cytoplasmic portion to regulate synaptic tiling. Based on the above-mentioned findings, we hypothesized that Semaphorin-Plexin signaling maintains synaptic tiling between DA8 and DA9 neurons by regulating not only Ras but also Rap small GTPase(s).

1.7 Rap small GTPases

1.7.1 Cycling of small GTPase

Small GTPases cycle between GTP- and GDP-bound conformations (Hall, 1990; Takai et al., 1992). As binary switches, once bound with GTP, they stay at an active state and interact with effectors to process downstream cell activities, whereas when bound with GDP they stay in an inactive form. The alteration between GTP- and GDP-bound states is mainly associated with two classes of regulators, GTPase activating proteins (GAPs) and GTP exchanging factors (GEFs). GAPs terminate the active state by promoting the hydrolysis of GTP; GEFs initiate the active state by switching GDP for GTP (Bos et al., 2007; Buday and Downward, 2008; Mitin et al., 2005; Vigil et al., 2010). The cellular or subcellular distribution and activation of GAPs and GEFs decide where and when small GTPases become active. Raps are members of a subfamily of the small GTPase superfamily, so we suggest that in *C. elegans*, PLX-1 functions as the GAP of RAP(s) in DA9 neuron to spatially regulate synaptic patterning.

1.7.2 The function of Rap small GTPases

The Rap family in humans includes Rap1a, Rap1b, Rap2a, Rap2b and Rap2c. There are three homologous *rap* genes in *C. elegans*: *rap-1* and *rap-3* show high identity to mammalian *Rap1b*, whereas *rap-2* shows high identity to *Rap2a* (Lundquist, 2006). The Rho proteins Rac1, CDC42 and RhoA were the earliest identified small GTPases that are involve in the regulation of the actin cytoskeleton dynamics in cell spreading, adhesion, polarization and pathfinding (Hall, 1992; Ken

Matsumoto et al., 1997; Nobes and Hall, 1995; Ridley and Hall, 1992; Ridley et al., 1992; Tapon and Hall, 1997). Later studies have identified more small GTPases participating in these complex activities, including Arfs (Klassen et al., 2010; Myers and Casanova, 2008) and Raps (sub-family members of Ras) (Di et al., 2015; Frische et al., 2007; Guo et al., 2016; Myagmar et al., 2005; Nonaka et al., 2008; Pannekoek et al., 2013; Park et al., 2013; Torti et al., 1999; Zhu et al., 2005).

Rap1 and Rap2 are believed to share a set of the same GAPs and GEFs, and Rap2 is believed to perform analogous functions to Rap1 (Ohba et al., 2000). However, the effector binding site of Rap2 is not completely identical to Rap1, so that Rap2 could interact with distinct effectors which do not interact with Rap1. This is supported by later findings in cultured rat hippocampal neurons, where among multiple initial neurites, Rap1B specifies one neurite, where it accumulates, to develop into an axon by activating and recruiting CDC42 to the tip of the polarized neurite. Rap2, on the other hand, promotes the retraction of the other neurites (Fu et al., 2007; Schwamborn and Püschel, 2004). Although reported to perform distinct functions, Rap1 and Rap2 could still share the same set of upstream regulators. Recently, PlexinA was reported to function as a GAP for Rap1 to regulate wound repair in *Drosophila* and zebrafish; moreover, Rap1 is also involved in the Semaphorin-Plexin pathway to modulate the pathfinding of the intersegmental nerve b motor axon in *Drosophila* (Yang et al., 2016; Yoo et al., 2016). So far, it is not known if Plexin regulates the activity of Rap2 as a GAP. In this study, I determined that the *rap-2* gene in *C. elegans* is involved in Plexin signaling to regulate synaptic

tiling of DA motor neurons. To the best of my knowledge, this is the first in vivo evidence that Rap2 acts in the Plexin pathway.

1.8 *mig-15*/*TNIK* kinase gene

1.8.1 Structural analysis of MIG-15

In this study, I found that the *C. elegans mig-15,* the homolog of the human *TNIK* gene, functions as an effector of *rap-2* to regulate synaptic tiling. TNIK (Traf2- and Nck-interacting kinase) belongs to the Ste20 subgroup of germinal center kinases (GCK) family (Fu et al., 1999). In mammals, TNIK and its paralogs mitogen-activated protein kinase 4 (MAP4K4) and Misshapen/NIKs-related kinase (MINK) were reported to activate the JNK pathway which can be activated by varieties of stress-inducing agents, such as UV irradiation, heat shock and osmotic shock (Ip and Davis, 1998). *mig-15* is the only *TNIK*, *MINK* and *MAP4K4* ortholog gene in *C. elegans* and shows the highest identity and similarity to *TNIK (Taira et al., 2004)*.

TNIK is mainly composed of three domains, a conserved N-terminal kinase domain, a variable intermediate proline-rich domain and a conserved C-terminal germinal center kinase homolog (GCKH, also called CNH) domain. Both C- and N-terminals of TNIK have kinase activity, and the proline-rich domain contains the binding site for NCK and Traf2/Traf6 (Fu et al., 1999; Shkoda et al., 2012). Moreover, TNIK specifically interacts with Rap2A, but not Rap1 and Ras, through its CNH domain, and the same specific interaction was also observed between worm RAP-2 and MIG-15 (Taira et al., 2004).

Interestingly, TNIK binds with both GTP- and GDP-bound Rap2A. Whereas the co-expression of Rap2A and TNIK in HEK293 cells did not enhance the TNIK induced JNK phosphorylation levels, indicating that the interaction of Rap2A and TNIK does not activate the JNK pathway to regulate the actin cytoskeleton activities. So far little evidence is found to support that the JNK pathway regulates actin dynamics (Taira et al., 2004; Weston and Davis, 2007). However, electrophysiology studies implicated that Rap2 stimulates JNK activity via interaction with TNIK and MINK2 to regulate the removal of synaptic AMPA receptors, which are widely expressed glutamate receptors important for study and memory activities in the central nervous system (Kielland et al., 2009; Zhu et al., 2005). More evidence is needed to clarify the relationship between Rap2/TNIK and JNK pathway.

1.8.2 Role of TNIK in actin cytoskeleton dynamics

TNIK is a kinase with diverse functions including a possible role as a psychiatric disease risk gene, an essential in gastric and colorectal cancer growth and it is required for B-Cell immune response induced by LMP1 oncoprotein (Shitashige et al., 2010; Shkoda et al., 2012; Wang et al., 2011; Yu et al., 2014). Moreover, TNIK/MIG-15 was reported to physically interact with PAT-3/integrin in *C. elegans* to regulate axon pathfinding. It may also be involved in the Wnt pathway to activate the expression of target genes by physically binding with two Wnt pathway components, beta-catenin and TCF4 (Chapman et al., 2008; Poinat et al., 2002; Shakir et al., 2006). In cultured cell lines, overexpression of TNIK induced actin cytoskeleton

rearrangement thereby disrupted cell spreading and induced cell rounding. This phenotype could be enhanced by the co-expression of Rap2A, whereas the overexpression of JNK did not induce cell rounding, suggesting that the TNIK-induced cell rounding is not through the activation of JNK pathway (Taira et al., 2004).

In vitro studies show that TNIK phosphorylates Gelsolin, which is one of the most potent actin-binding proteins. Gelsolin severs actin filaments and caps the barbed end of segmented actin, which suggests the possibility that TNIK induces actin rearrangement through phosphorylating Gelsolin (Fu et al., 1999; Sun et al., 1999; Taira et al., 2004; Tomas et al., 2006; Yin and Stossel, 1979). Further studies, especially in vivo evidence will be needed to identify the downstream targets of TNIK to connect its activity with actin rearrangement.

1.9 Aims of this thesis

In this thesis, the DA class motor neurons of *C. elegans* are used as a model system to study the roles of *rap-2* and *mig-15* genes in the regulation of synaptic tiling, and the genetic relationships among *plx-1*, *rap-2* and *mig-15* are addressed.

The specific studies described in this thesis are:

1. Characterizing the role of *rap-2* gene in synaptic tiling (Chapter 3).
2. Identifying the role of *mig-15* gene in synaptic tiling (Chapter 4).
3. Describing the relationships among *plx-1*, *rap-2* and *mig-15* (Chapter 5).

Chapter 2: Materials and Methods

2.1 Strains and genotype validation

2.1.1 Strains and worm culture

N2 wild-type, ST36 *plx-1 (nc36)IV*, VC14 *rap-2 (gk11)V*, NJ490 *mig-15 (rh148)X*, NJ290 *mig-15 (rh80)X*, NJ834 *mig-15 (rh326)X*, UJ387 *rap-2 (miz16)V*, UJ388 *rap-2 (miz17)V*, UJ401 *rap-2 (miz18)V*, UJ402 *rap-2 (miz19)V*, UJ403 *rap-2 (miz20)V*, TZ181 *rap-1 (pk2082)IV*, VC3737 *rap-3 (gk3975)IV*, TV14517 *wyIs446*, TV14856 *wyIs524* and TV1229 *wyIs85* were used for experiments. Worms were fed with *OP50 E. coli* dropped onto 10 ml nematode growth medium agar in 60 mm*15 mm Petri plates at 20 ^{o}C (Brenner, 1974). UJ387, UJ388, UJ401, UJ402 and UJ403 are from Mizumoto lab, University of British Columbia (UBC) generated by CRISPR/Cas9 genome editing method; VC3737 is from Moerman lab, UBC, generated by CRISPR/Cas9; TV14517, TV14856 and TV1229 are from Shen lab, Stanford University; and all the rest strains are ordered from the Caenorhabditis Genetics Center.

2.1.2 DNA extraction and polymerase chain reaction

The genotype of each mutant allele was validated by electrophoresis of amplified DNA fragments after polymerase chain reaction (PCR).

DNA extraction: ~20 worms from one candidate population were collected into PCR tube and washed by M9 buffer (3 g KH_2PO_4, 6 g Na_2HPO_4, 5 g NaCl, 1 ml 1 M

$MgSO_4$ and H_2O to 1 liter, sterilized by autoclaving). M9 buffer was removed by pipetting and leaving washed worms at the bottom. Twenty µl of lysis buffer (20 mM pH7.5 Tris, 50 mM EDTA, 200mM NaCl and 0.5% SDS) and proteinase K (100 µg /ml) were added into the PCR tube, mixed and spun down properly. Worms were lysed at 65 ^{o}C for 1 hour followed by 95 ^{o}C proteinase K inactivation for 15 minutes. DNA released from worm lysis was used immediately as PCR templates or stored at -20 ^{o}C.

PCR reaction: Dream Tap polymerase and buffer (Thermo Fisher Scientific, USA, catalog #Ep0703) were used for PCR. The recipe and protocol for PCR were used according to the instructions of Dream Taq polymerase on Thermo Fisher website.

Primers (synthesized by Thermo Fisher Scientific, USA) for genotype validation:

rap-2 (gk11)

Sense primer: 5'-TCT CAT CTC CAT CGT CGT TCC TGC -3'

External antisense primer: 5'- GAG GGA GTT CAA AGT GGT CGT TC -3'

Inner antisense primer: 5' - TCC ATT CAC TGA ATG TTC CGC - 3'

plx-1 (nc36)

Sense primer: 5' - CTT CGA GAG CCC CCC TCA TTC TTG ATG – 3'

External antisense primer: 5' - GAT GAG AGA AAG CCA ACG TCT CAA G - 3'

Inner antisense primer: 5' - CCG GCA CAC GTT AAA CTA GTG CTA CCG - 3'

rap-2 (miz17, miz18, miz19, miz20)

Sense wild-type primer: 5'- AAG TGG TCG TTC TGG GTA GT - 3'

Sense primer with mutations: 5' – AAG TCG TGG TTC TTG GTT CA - 3'

Antisense primer: 5' - CTT GTT AAC TTC AGG TTC CAC TGG G - 3'

rap-3 (gk3975)

Sense primer: 5' - CTT GTT AAC TTC AGG TTC CAC TGG G - 3'

Antisense primer: 5' - GTT CTG GTT GAG CCT TGC ACT AGT C - 3'

2.2 Plasmids and construction

C. elegans expression clones were made in a derivative of pPD49.26 (A. Fire), the pSM vector (kind gift from S. McCarroll and C. I. Bargmann). The following constructs were used and transgenes were generated using standard microinjection method (Mello et al., 1991):

pSM388 (*Punc-4::rap-1 G12V)*, pSM409 (*Punc-4::rap-2 G12V)*, pCM32 (*Punc-4c::rap-1)*, pSM411 (*Punc-4c::rap-2)*, pSM397 (*Pmig-13::rap-2)*, pSM410 (*Punc-129::rap-2)*, pSM398 (*Phlh-1::rap-2)*, pCM31 (*Punc-4c::Rap2a)*, pCM33 (*Prap-3::novo2)*, pSM63 (*Pmig-13:: myr-mCherry (myristolated mCherry))*, pCM28 (*Pmig-13::mcherry::rap-2 G12V),* pCM29 (*Pmig-13::mcherry::rap-2 S17A)*, pCM30 *(Punc-4c::mig-15)*, pCM42 *(Punc-129::mig-15)*, pCM40 *(Pmig-13::mig-15)*, pCM26 *(Pflp-13:;mig-15),* pCM45 *(pSM::mig-15),* pCM39 (*Pitr-1::mig-15::novo2).*

For all vectors, *SphI* and *AscI* restriction sites (*SphI* and *AscI* enzymes and digestion buffers from New England Biolabs, USA) were used for promoter insertion; *AscI* and *KpnI (KpnI* enzyme and digestion buffer from New England Biolabs, USA) restriction sites were used for cDNA or genomic coding DNA insertion. Plasmid and DNA fragments were digested at 37 ^{o}C for a few hours followed by electrophoresis separation on 1% agar gels made with 1xTBE buffer (89 mM PH7.6 Tris, 89 mM boric acid and 2 mM EDTA). The desired fragments were cut from the 1% agar gel and purified by a gel purification kit (Thermo Fisher, USA, catalog #K0692). T4 DNA ligase (New England Biolabs, USA, catalog #M0208L) was used for the ligation of digested and purified DNA fragments at 16 ^{o}C overnight. Turbo *E. coli* competent cells (New England Biolabs, catalog #C2984H) were used for plasmid transformation and amplification. Competent *E. coli* cells were thawed on ice from -80 ^{o}C, incubated with the constructed plasmid for 30 minutes on ice, heat-shocked for 30 seconds at 42 ^{o}C, put back immediately on ice for a 5 minutes incubation and applied on ampicillin selection medium agar in 100 mm*15 mm Petri dishes. Single colonies were picked from the agar surface after 12 hours culture at 37 ^{o}C and cultured in 4 ml ampicillin liquid culture medium for 12 hours in a shaker at 37 ^{o}C. Amplified *E. coli* were then collected by centrifugation (14000 rpm, 2 minutes) and lysed for plasmid extraction and purification (plasmid purification kit was from Thermo Fisher, catalog #K0503). The sequence of the inserted DNA fragments was confirmed by Sanger sequencing (NAPs unit, UBC, website address: https://sequencing.ubc.ca). Information for cDNAs and genomic coding sequence see Wormbase (website address: http://www.wormbase.org/#012-34-5).

2.3 CRISPR/Cas9 genome editing

rap-2(miz17)V, rap-2(miz18)V, rap-2(miz19)V and *rap-2(miz20)V* were generated using the co-CRISPR/Cas9 method (Kim et al., 2014). *dpy-10* co-CRISPR marker was used for selecting candidate animals (Arribere et al., 2014; Kim et al., 2014). Vectors for sgRNA and Cas9 were obtained from Addgene (USA) (Friedland et al., 2013). The guide RNA targeting *rap-2* was designed using MIT CRISPR design tool (http://crispr.migt.edu.8079/). Cas9 plasmid (50 ng/µl), guide RNA plasmids (50 ng/µl for each) and homologous repair template plasmid (50 ng/µl) were properly mixed and centrifuged (14000 rpm, 10 minutes) and micro-injected together into the gonads of N2 hermaphrodites (Dickinson et al., 2013).

Sequence of sgRNA targeting *rap-2:*

5’ - g TAG TGG AGG TGT CGG AAA AT - 3’

Homologous repair template induced silent mutations and G12V:

5’ ~ 500bp homologous flanking sequence

-ATGAGGGAGTTCAAAGTcGTgGTTCTgGGTagtGttGGTGTCGGAAAATCG-

500bp homologous flanking sequence ~3’

Homologous repair template induced silent mutations and S17A:

5’ ~ 500bp homologous flanking sequence

-ATGAGGGAGTTCAAAGTcGTgGTTCTgGGTagtGGAGGTGTCGGAAAAgCG-

500bp homologous flanking sequence ~ 3’

2.4 Quantitative PCR

Quantitative PCR (qPCR) was used to test the *rap-2* gene expression level of N2 and CRISPR/Cas9 method generated *rap-2* mutants *(miz16, miz17, miz18, miz19, miz20)*. Ten well-feed larvae 4 stage worms of each genotype were picked and left on 60 mm*15 mm Petri plate for populating. Fully populated and well-feed worms were washed with M9 buffer, collected by centrifuge (14000 rpm, 10 minutes) and completely frozen at -80 ^{o}C. RNA library of frozen worms was extracted by using the RNA extraction kit (Thermo Fisher, USA, catalog #0731). Extracted RNA was diluted to 100 ng/µl as the template for reverse transcription-qPCR (RT-qPCR) by using dye-based Luna Universal One-Step RT-qPCR kit (New England Biolabs, USA, catalog #E3005). Recipe and protocol were used according to the instructions on the company website. Bio-Rad CFX384 Touch™ Real-Time PCR Detection System was used to detect gene expression level. *cdc-42* was used as internal reference gene (Goh et al., 2014). Primers (synthesized by Thermo Fisher Scientific, USA) used for qPCR:

rap-2

Sense primer: 5’ - CGT TGA CGG TGC AAT TTG TCA G - 3’

Antisense primer: 5’ - CCT GCA GTC TCC AGA ATT TCC AC - 3’

cdc-42

Sense primer: 5’ - CTG CTG GAC AGG AAG ATT ACG - 3’

Antisense primer: 5’ - CTC GGA CAT TCT CGA ATG AAG - 3’

2.5 Confocal Microscopy

Carl Zeiss LMS800 confocal microscope (Carl Zeiss, Germany) in Mizumoto lab was used to capture the image in live animals with fluorescently tagged proteins. 488 nm and 568 nm lasers were used to excite GFP and mCherry signal respectively. Worms were immobilized on 2% agarose pad using a mixture of 7.5 mM levamisole (Sigma-Aldrich, USA) and 0.225 M BDM (2, 3-butanedionemonoxime) (Sigma-Aldrich, USA). The fluorescent images were obtained by 63X or 40X oil lenses (Carl Zeiss, Germany). Zen blue edition version 2.1 was used for measurement and image processing.

2.6 Statistics

Prism7 (GraphPad Software, USA) was used for data processing. Tukey correction and Dunnet's test one-way ANOVA methods were used for comparison among more than three experimental groups. Two tails student's t-test was used to test the difference between two experimental groups. Data were represented as mean ± SEM (standard errors of the mean). *, ** and *** were used to represent when P value is <0.05, <0.01 and <0.001 respectively.

2.7 Image processing

For the alignment of the images of the DA9 synaptic domain, DA9 commissure was used as a landmark, ImageJ (NIH, USA) was used to straighten the selected area, Adobe Photoshop was used to crop straightened areas into same width and height and Microsoft PowerPoint was used to seam and align 20 cropped images.

Chapter 3: The Role of the *rap-2* Gene in Synaptic Tiling

3.1 *rap-2* is responsible for synaptic tiling

3.1.1 Constitutively GTP-bound RAP-1 and GTP-bound RAP-2 both induce synaptic tiling defects

I reasoned that as a RapGAP, PLX-1 defines the synaptic tiling border by switching GTP-RAP to GDP-RAP, so that GDP-RAP accumulates at the synaptic border to restrict the extension of the synaptic domain. As mentioned above, *rap-1* and *rap-3* genes are both homologs of mammalian *Rap1b,* and the *C. elegans rap-2* shows high identity to mammalian *Rap2a*. I first tested if the expression of the constitutive GTP bound RAP-1 and RAP-2 can mimic the synaptic tiling defect of *plx-1* mutants in DA neurons. The length of DA8/DA9 overlap was measured and quantified. DA8/DA9 overlap is defined from the most anterior DA9 pre-synapse to the most posterior DA8 pre-synapse of tested animals. A glycine to valine substitution on the twelfth codon (G12V) keeps both RAP-1 and RAP-2 in a constitutively GTP-bound stage (Fu et al., 2007). As expected, the DA neurons' cell-specific expression of either *rap-1 (G12V)* or *rap-2 (G12V)* in wild-type animals both mimicked the phenotype of *plx-1* mutant (Figure 3.1 A, B, C, D, E). Since the cell-specific expressions of *rap-1 (G12V)* and *rap-2 (G12V)* were induced by extrachromosomal (Ex) transgenic arrays (composed of cell-specific promoter and related cDNA), which are less stable than endogenous gene expression, the DA8/DA9 overlap fluctuated among each tested animal (Figure 3.1 E) (Stinchcomb et al., 1985). In this study, similar circumstances happened to other Ex expression tests as well, which

won't be discussed hereafter. Because Rap1 and Rap2 were reported to share the same sets of GAPs and GEFs, and Rap1 was found to be regulated by Plexin in *Drosophila* (Ohba et al., 2000; Yang et al., 2016; Yoo et al., 2016), it is not surprising that GTP-RAP-1 and GTP-RAP-2 both disturbed the Semaphorin-Plexin signaling transduction in DA neurons.

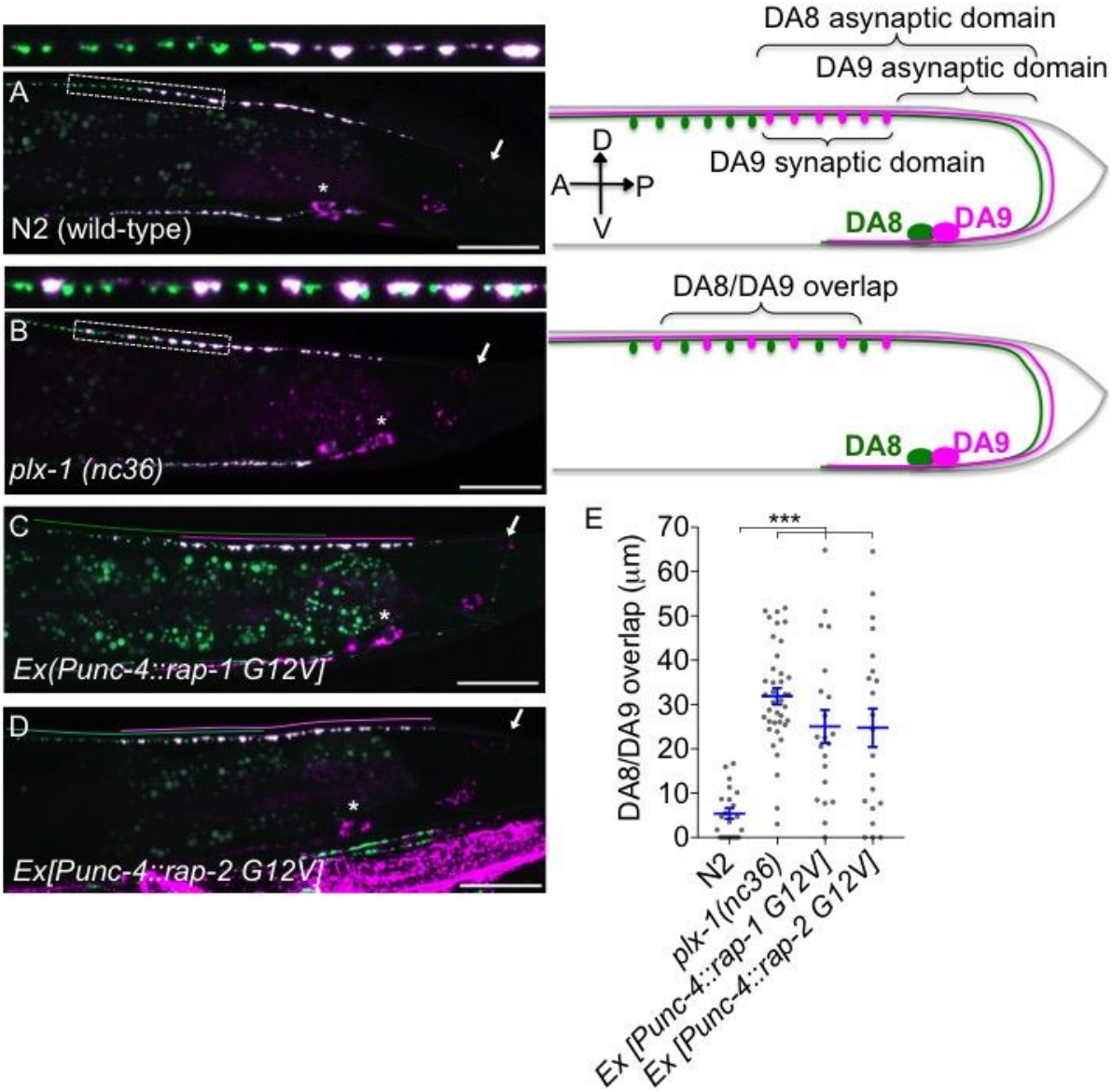

Figure 3.1 RAP-1 G12V and RAP-2 G12V both induced synaptic tiling defects. (A) Representative image and schematic of the DA8/DA9 synaptic tiling, the three parameters used in this study are shown. “D”, “V”, “A” and “P” represent dorsal, ventral, anterior and posterior respectively. (B) Representative image and schematic of the tiling defect of *plx-1* mutant. DA8/DA9 synaptic overlap in the dotted frame is magnified and shown. (C-D) Representatives of synaptic tiling defect induced by RAP-1 G12V (C) and RAP-2 G12V (D). Magenta line delineates DA9 synaptic domain and green line delineates DA8 synaptic domain. (E) Quantification of the overlap between DA8/DA9 synaptic domains at the middle Larvae 4 (L4) stage, each dot represents a single animal. Error bars represent SEM; ***$p < 0.001$ (ANOVA/Dunnett). Scale bar represents 20 µm. White asterisk and arrow indicate cell body and axon respectively.

3.1.2 *rap-2* mutants show synaptic tiling defects

Because the small GTPases function as a binary switch to associate with downstream effectors to regulate cell activities, I asked the question if endogenous *rap* genes are required to maintain synaptic tiling. I next observed if worms show synaptic tiling defect in the absence of *rap* genes. For this purpose, I picked a null allele (*pk2082*) of the *rap-1* gene that contains a nonsense mutation in the middle of the transcript, a null allele (*gk11*) of the *rap-2* gene that contains a large deletion within the coding sequence, and a null allele (*gk3975*) of the *rap-3* gene that contains a deletion covering the start codon and its flanking sequence. To my surprise, only *rap-2* mutants show obvious synaptic tiling defect (Figure 3.2 B and D), whereas *rap-1* and *rap-3* mutants show no significant differences compared to wild-type animals (Figure 3.2 A, C and D). Because *rap-1* mutants show mild phenotypes,

I then quantified the DA8/DA9 overlap of the *rap-1*;*rap-2* double mutants, which do not show an enhanced effect (Figure 3.2 D). Consistent with this result, a GFP reporter was used to examine the expression pattern of the three *rap* genes, and only the *rap-2* gene showed detectable expression in DA neurons (Figure 3.2 E, F and G). Based on the observations of this section, *rap-2* might be the only *rap* gene involved in the regulation of synaptic tiling between DA8 and DA9.

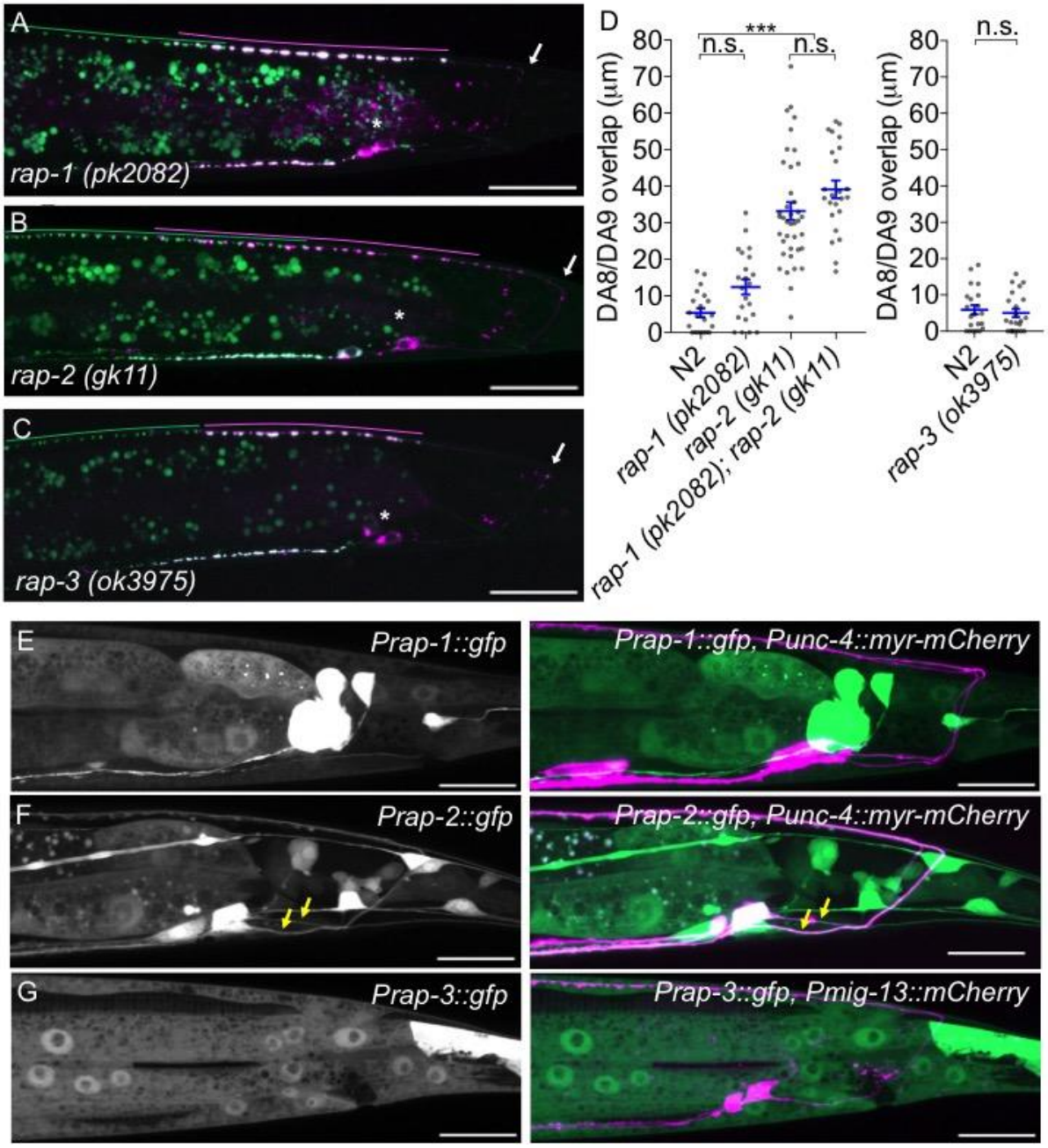
A
rap-1 (pk2082)
B
rap-2 (gk11)
C
rap-3 (ok3975)
D
DA8/DA9 overlap (μm)
n.s.
***
n.s.
N2
rap-1 (pk2082)
rap-2 (gk11)
rap-1 (pk2082); rap-2 (gk11)
n.s.
rap-3 (ok3975)
E
Prap-1::gfp
Prap-1::gfp, Punc-4::myr-mCherry
F
Prap-2::gfp
Prap-2::gfp, Punc-4::myr-mCherry
G
Prap-3::gfp
Prap-3::gfp, Pmig-13::mCherry

Figure 3.2 The *rap-2* gene is required for DA8/DA9 synaptic tiling and expressed in DA neurons.

(A-C) Representative images of the synaptic patterns in DA8 and DA9 of *rap-1* (A), *rap-2* (B) and *rap-3* (C) mutants, the arrow denotes DA9 commissure. (D) Quantification of DA8/DA9 synaptic overlap, each dot represents a single animal. Error bars represent SEM; ***$p < 0.001$, n.s., not significant (ANOVA/Dunnett and student t-test). Scale bar represents 20μm. (E-G) Representative images of the expression patterns of *rap-1* (E), *rap-2* (F) and *rap-3* (G) genes. Yellow arrows in panel F denote DA8 and DA9 axons. Scale bar represents 20 μm. White asterisk and arrow indicate DA9 cell body and axon respectively.

3.1.3 Synaptic tiling defect of *rap-2* mutant is caused by the extension of DA8 and DA9 synaptic domains

The DA9 synaptic domain and the DA8 asynaptic domain were measured to determine if they both extend in *rap-2* mutants. The DA9 synaptic domain is defined as the most posterior to the most anterior DA9 dorsal punctum; the DA8 asynaptic domain is defined as the synapse free domain from DA8 axon commissure to the first posterior DA8 dorsal punctum (see schematics in Figure 3.1 A). Similar to *plx-1* mutants, the DA8/DA9 synaptic overlap in *rap-2* mutants is caused by the posterior extension of DA8 and DA9 synaptic domains into each other's territory (Figure 3.3 A and B).

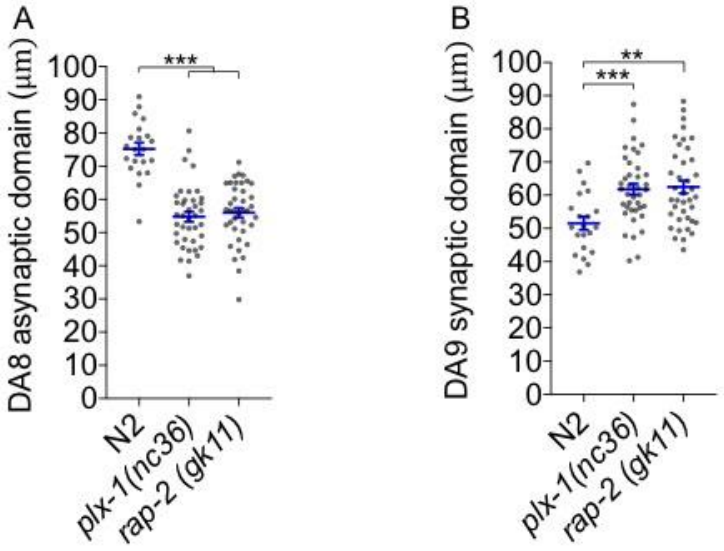

Figure 3.3 DA8 and DA9 synaptic domains are both extended in *rap-2* mutants.

(A-B) Quantification of the asynaptic domain of DA8 (A) and synaptic domain of DA9 (B), each dot represents a single animal. Error bars represent SEM; *** $p < 0.001$, ** $p < 0.01$, n.s., not significant (ANOVA/Dunnett).

3.2 *rap-2* genetically acts in the same pathway with *plx-1*

Since *rap-2* and *plx-1* mutants show the same level of synaptic tiling defect (shown in figure 3.3), I next asked whether these two genes genetically act in the same pathway. To answer this question, *plx-1* and *rap-2* double mutants were generated to test if the synaptic tiling defect is enhanced compared to plx-1 and rap-2 single mutants. The DA8/DA9 overlap is not enhanced in the double mutants, which supports that *plx-1* and *rap-2* genetically act in the same pathway to regulate synaptic tiling (Figure 3.4).

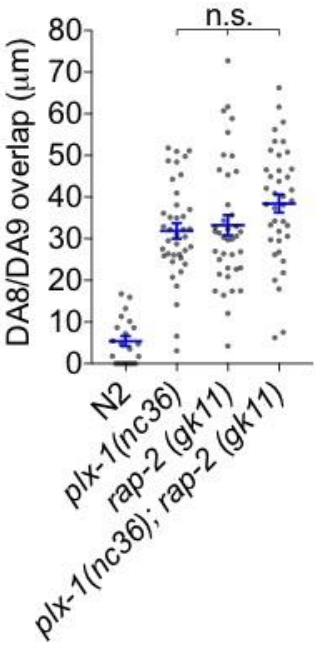

Figure 3.4 ***plx-1* and *rap-2* genetically act in the same pathway.**
Quantification of DA8/DA9 synaptic overlap, each dot represents single animal. Error bars represent SEM; *** $p < 0.001$, n.s., not significant (ANOVA/Tukey).

3.3 *rap-2* acts cell autonomously in DA neurons

In the previous study, Mizumoto found that *plx-1* acts cell autonomously in DA9 to maintain synaptic tiling (Mizumoto and Shen, 2013b). So I reasoned that if PLX-1 functions as a GAP of RAP-2, then *rap-2* should also act cell autonomously in DA neurons. To test this assumption, a series of cell-specific rescue experiments were performed on *rap-2* mutants to determine whether *rap-2* functions autonomously in DA9.

The expression of *rap-2* complementary DNA (cDNA) driven by a body muscle wall specific promoter *hlh-1* does not restore the clear boundary between DA8 and DA9

synaptic regions, indicating that *rap-2* does not act in the postsynaptic muscles to maintain DA synaptic tiling (Figure 3.5 A and G) (Krause et al., 1990). Moreover, the specific *rap-2* cDNA expression driven by the *unc-129* promoter in DB class motor neurons, which also innervate on the dorsal muscle wall, does not rescue the DAs synaptic tiling defect, supporting that *rap-2* does not function in DB neurons to maintain DA synaptic tiling (Figure 3.5 B and G) (Klassen and Shen, 2007; White et al., 1976). As expected, the DAs specific RAP-2 expression, but not RAP-1 expression, recovered synaptic tiling (Figure 3.5 C, F, G, H and I). DA9 specific RAP-2 expression (driven by *mig-13* promoter) rescued the extended DA9 synaptic domain, but not the expansion of DA8 synaptic domain (Figure 3.5 E, G, H and I), supporting that *rap-2* regulates synaptic tiling in a cell autonomous manner (Klassen and Shen, 2007; Miller and Niemeyer, 1995). These results are consistent with the idea that *rap-2* acts in DAs to regulate synaptic tiling, whereas *rap-1* does not participate in this process. Furthermore, the human *Rap2a* cDNA, which shows 60% also rescued *rap-2* mutants, indicating the conserved function of *rap-2* across species (Figure 3.5 D and G).

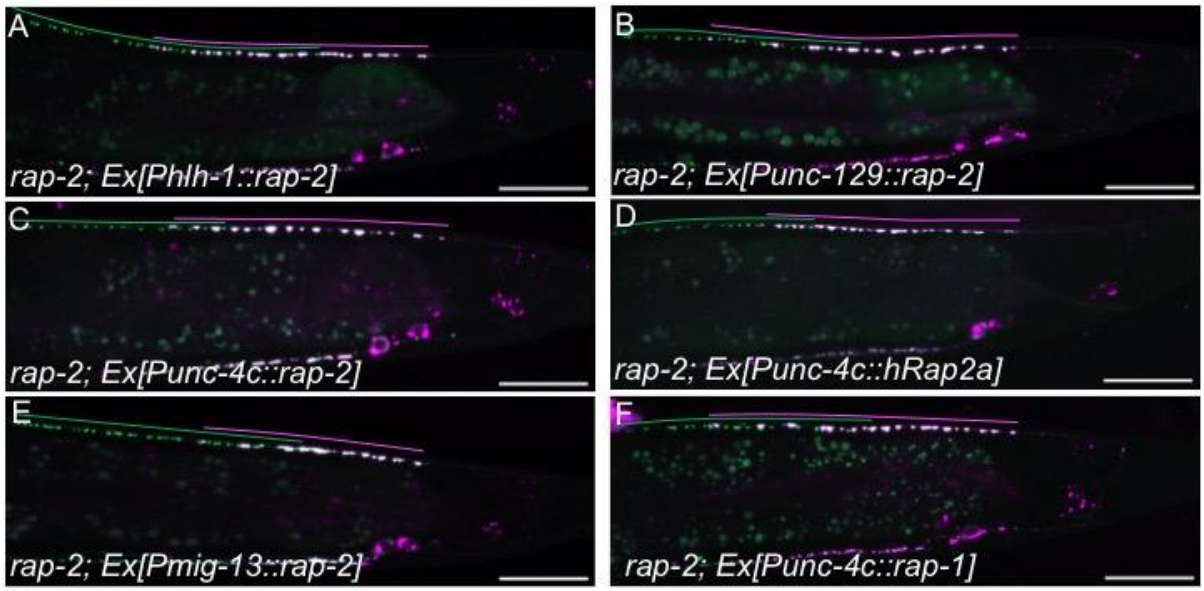

G

```
Rap2A MREFKVVVLGSGGVGKSALTVQFVSSTFIEKYDPTIEDFYRKEIEVDGQPSVLEILDTAG  60
      MRE+KVVVLGSGGVGKSALTVQFV+ TFIEKYDPTIEDFYRKEIEVD  PSVLEILDTAG
RAP-2 MREYKVVVLGSGGVGKSALTVQFVTGTFIEKYDPTIEDFYRKEIEVDSSPSVLEILDTAG  60

Rap2A TEQFSSMRDLYIKNGQGFVVVYSITSQQTFHDIRNMKEQIVRVKGSENVPILLVGNKCDL  120
      TEQF+SMRDLYIKNGQGF++VYS+ +QQ+F DI+ M++QI+RVK  E VP++LVGNK DL
RAP-2 TEQFASMRDLYIKNGQGFILVYSLVNQQSFQDIKPMRDQIIRVKRYEKVPVILVGNKVDL  120

Rap2A SHQRQVRSEEGLALAESWSCPFTECSAKNNQNVNVTFAEIVREMNYVQNKSRQSKSCCS  179
        +R+V S EG ALAE W CPF E SAK+   V+  FAEIVR+MNY     +    CCS
RAP-2 ESEREVSSSEGRALAEEWGCPFMETSAKSKTMVDELFAEIVRQMNYAAQPDKDD-PCCS  178
```

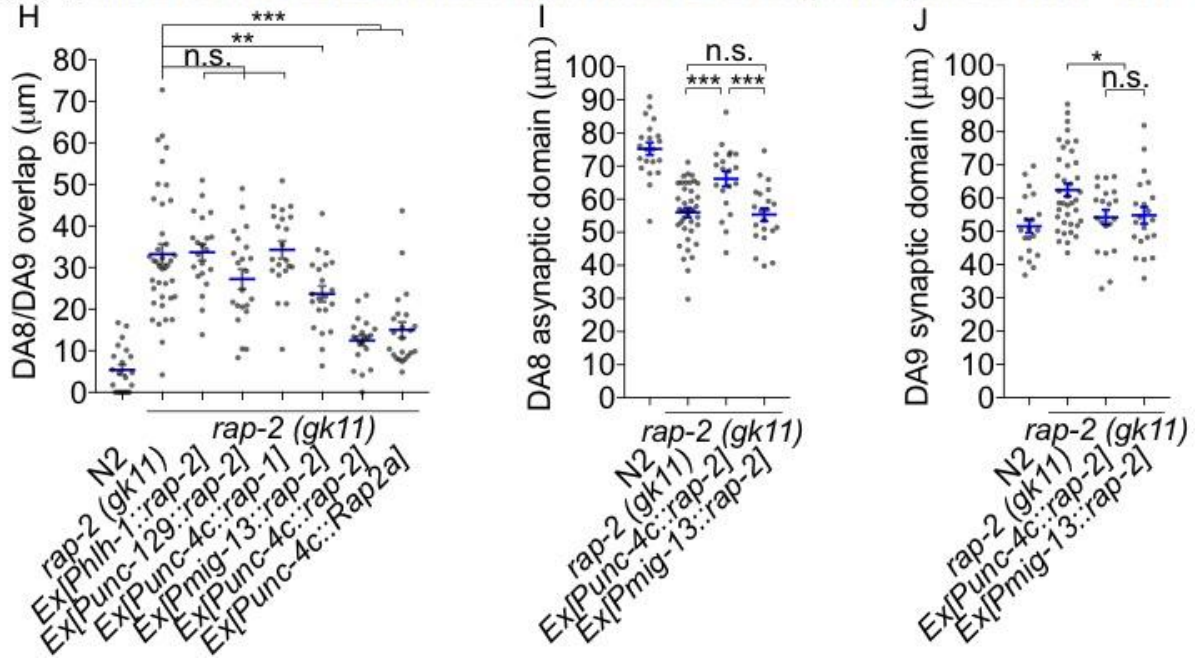

Figure 3.5 *rap-2* acts cell autonomously in DAs.

(A-F) Cell-specific rescue in *rap-2* mutants: body wall muscle (A), DBs (B), DAs (C) and DA9 (E) rescue using *rap-2* cDNA; DAs rescue using human *Rap2a* cDNA (E); DAs rescue using *rap-1* cDNA (F). (G) Comparison between human Rap2A and C. elegans RAP-2 proteins. (H-J) Quantification of DA8/DA9 overlap (H), DA8 asynaptic domain (I) and DA9 synaptic domain (J), each dot represents single animal. Error bars represent SEM; *** $p < 0.001$, ** $p< 0.01$, * $p< 0.05$, n.s., not significant (ANOVA/Dunnett). Scale bar represents 20 µm.

3.4 The cycling of RAP-2 is required for synaptic tiling

3.4.1 Generating constitutively GTP-bound *rap-2* and GDP-bound *rap-2* mutants

Given that wild-type animals expressing DAs specific *rap-2 (G12V)* and *rap-2* null mutants both show synaptic tiling defects, I asked if GTP- and GDP-bound RAP-2 are both required by synaptic tiling. To test this possibility, three constitutively GTP-bound (G12V) *rap-2* mutants (*miz16, miz17, miz18*) and two constitutively GDP-bound (S17A) *rap-2* mutants (*miz19, miz20*) were acquired by using CRISPR/Cas9 genome editing. The induced mutations were all confirmed by Sanger sequencing (Figure 3.6 A). The *rap-2* mRNA levels of each mutants strain are comparable with wild-type animals, which were confirmed by qPCR by using *cdc-42* as a reference gene (Figure 3.6 B).

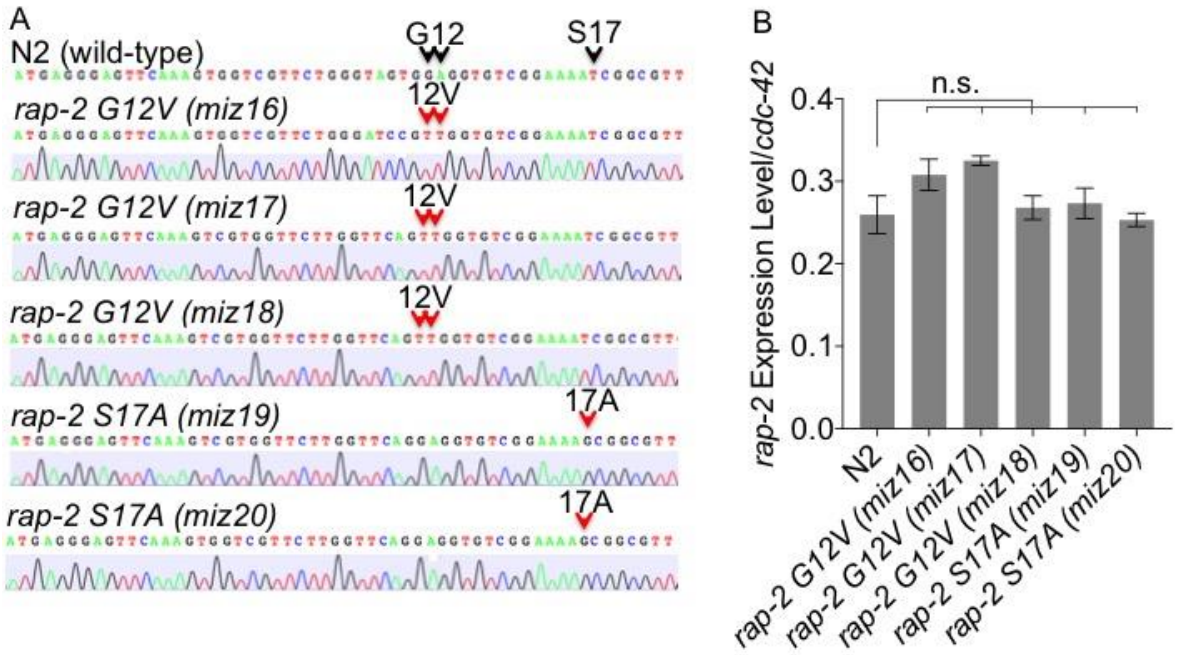

Figure 3.6 The sequence and unchanged expression levels of five *rap-2* mutants generated by CRISPR/Cas9.

(A) Sequence comparison between wild-type and the five *rap-2* mutants. Black arrowhead denotes wild-type sequence and red arrowhead denotes mutant sequence. (B) Quantification of qPCR, average of 3 independent qPCR reactions are shown. Error bars represent SEM; n.s., not significant (ANOVA/Dunnett).

3.4.2 Both GTP-RAP-2 and GDP-RAP-2 are required to regulate synaptic tiling

I then observed and compared the DA8/DA9 synaptic overlap of these mutants. All five mutant lines show synaptic tiling defects and none of them enhances the phenotype of the *plx-1* mutants (Figure 3.7 A and B). These results further support the idea that *rap-2* and *plx-1* genetically act in the same pathway and RAP-2 cycles between GTP/GDP binding status as a binary switch to dynamically regulate the synaptic tiling of DAs.

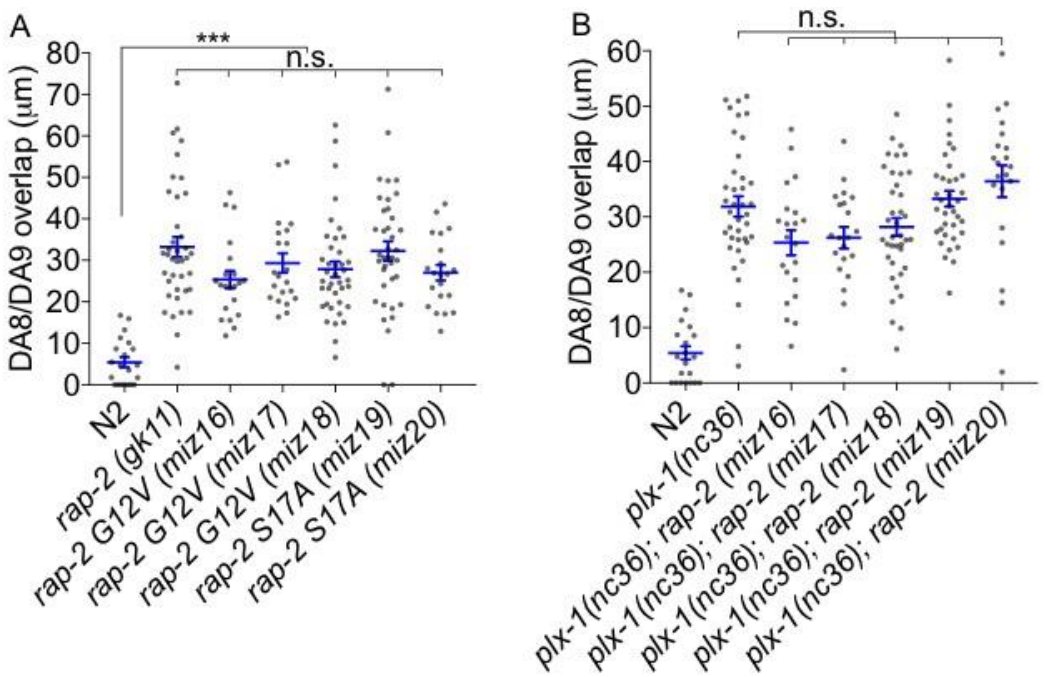

Figure 3.7 Constitutively GTP- and GDP-bound *rap-2* mutants show synaptic tiling defects and do not enhance *plx-1*.

(A) Quantification of DA8/DA9 overlap of *rap-2* mutants. (B) Quantification of DA8/DA9 overlap of *plx-1;rap-2* double mutants. Each dot represents single animal. Error bars represent SEM; *** $p < 0.001$, n.s., not significant (ANOVA/Tukey).

3.5 Detecting GTP-RAP-2 and GDP-RAP-2 at the subcellular level

I next determined the subcellular localization of GTP- and GDP-bound RAP-2. Because many lines of evidence have shown that small GTPases are spatially regulated by GAPs and GEFs to participate in cell activities (Bos et al., 2001; F et al., 1991; Fu et al., 2007; Ohba et al., 2000; R et al., 1996), I predicted that GTP- and GDP-RAP-2 are localized to distinct subcellular regions to regulate synapse patterning. To test this idea, GTP- and GDP-RAP-2 were tagged with mCherry fluorescent protein and their localization was examined in DA9 neuron. For this

purpose, GFP tagged RAB-3 was co-expressed to visualize DA9 synapses. mCherry-GTP-RAP-2 is consistently diffused across axon and synapses (Figure 3.8 A), whereas mCherry-GDP-RAP-2 is detected to be punctate at the peri-synapse domains (Figure 3.8 B). These results support the speculation that GTP- and GDP-RAP-2 are spatially regulated.

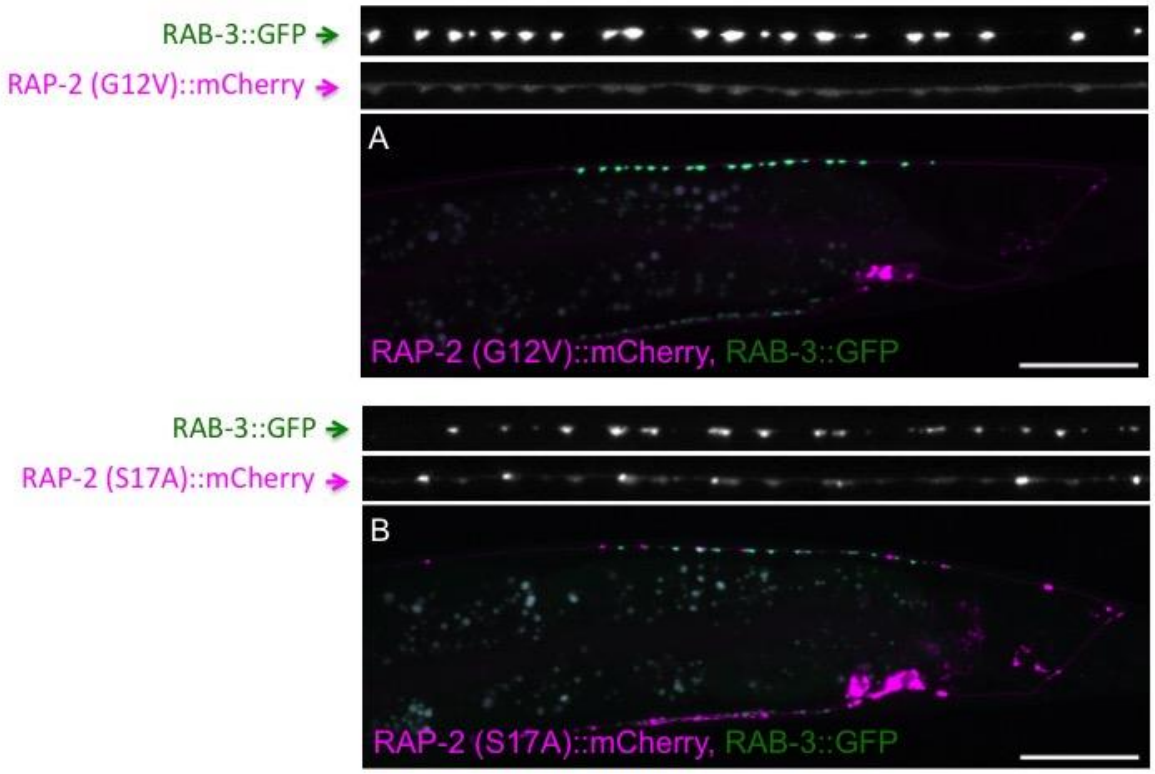

Figure 3.8 Localization of GTP-RAP-2 and GDP-RAP-2.

(A) Representative image of GTP-RAP-2 localization, RAB-3::GFP and RAP-2(G12V)::mCherry in synaptic domain are magnified on top. (B) Representative image of GDP-RAP-2 localization, RAB-3::GFP and RAP-2 (S17A)::mCherry in synaptic domain are magnified on top. Scale bar represents 20 µm.

3.6 Discussion

Due to the high identity of *Rap1* and *Rap2* genes (60%), they have been found to share the same set of GEFs and GAPs (Ohba et al., 2000). Moreover, they were reported to act either antagonistically to regulate barrier resistance of human epithelial cells (Pannekoek et al., 2013) or coordinately to activate human neutrophils (Maridonneau-Parini and Gunzburg, 1992). It is possible that once being activated they regulate multiple activities by binding with different sets of downstream effectors according to the complex stimulations from the surrounding microenvironments. This idea is supported by the evidence that the effector binding sites (amino acids 32-40) of Rap1 and Rap2 are not identical, as in Rap1 the 39th amino acid is serine, while in Rap2 it is phenylalanine (Myagmar et al., 2005; Taira et al., 2004); two Rap2 specific GEFs, RasGEF1A and RasGEF1B, were reported to discriminate Rap1 and Rap2 according to this single amino acid site (Yaman et al., 2009). The compartmentalization differences of Rap1 and Rap2 also explain why they perform distinct regulatory roles (Fu et al., 2007; Nancy et al., 1999). For example, activated Ras, Rap1 and Rap2 are all able to interact with three RalGEFs: RalGDS, RGL and Rlf. Ras and Rap1 both induce Ral activation through activating these GEFs, whereas Rap2 re-localizes these GEFs from the cell membrane into the endoplasmic reticulum without changing Ral's activity, supporting that Rap1 and Rap2 send distinct signals to their effectors to execute different cell activities (Nancy et al., 1999).

In my study, it appears that D8 and DA9 motor neurons selectively express *rap-2* rather than *rap-1* or *rap-3* to specifically regulate synaptic tiling. According to my experiment results, the expression of *rap-1* and *rap-2* mutants (*G12V)* in DAs of wild-type animals were both able to disturb the clear boundary between DA8 and DA9 synaptic domain, whereas the absence of neither *rap-1* nor *rap-3* causes or enhances detectable synaptic tiling defect. The fact that RAP-1 expression in DAs did not rescue the DA8/DA9 overlap suggests that although GTP-RAP-1 interferes the upstream signal (Semaphorin-Plexin signaling in this case), RAP-1 is not able to replace the role of RAP-2 to process specific downstream activities and regulate DAs' synaptic tiling. However, it is possible that *rap-1* and *rap-3* are involved in Semaphorin-Plexin pathway in other tissues or cell types such as hypodermal and vulva cells (Frische et al., 2007b; Fujii et al., 2002; Liu et al., 2005; Zand et al., 2011).

My surprise for the *rap-2* study is that not only do *rap-2 (G12V)* mutants show synaptic tiling defects, but also *rap-2 (S17A)* mutants. Moreover, neither of them enhances the severity of *plx-1* mutants, indicating that GTP- and GDP-RAP-2 regulate synaptic tiling in the same pathway. Furthermore, I found that GTP- and GDP-RAP-2 localize at distinct subcellular localizations, supporting the idea that the activities of RAP-2 are spatially regulated by GAP(s) and GEF(s), in which case PLX-1 functions as a GAP to promote the formation of GDP-RAP-2 at the DA9 synaptic border to inhibit the over-extension of DA9 synapses.

I was not able to identify the specific GEF(s) for RAP-2 in the regulation of synaptic tiling. None of the mutants of RAP-GEF candidate genes, including *pxf-1/RapGEF2*, *epac-1/Epac1*, *Y34B4A.4/RapGEF1* and *rgef-1/RasGRP*, shows noticeable synaptic tiling defects (data not shown) (Berkel et al., 2005; Shaye and Greenwald, 2011; Tada et al., 2012). On this point, I could not provide more evidence of how the formation of GTP-RAP-2 is spatially regulated by GEF(s). However, it is possible that GTP-RAP-2 is diffused across DA9 axon and synapses because of the redundancy of GEF(s). I then moved on to look for and characterize downstream effectors of RAP-2, MIG-15, which will be addressed in next chapter.

3.7 Conclusions

In the section on my *rap-2* study, the *rap-2* gene, not *rap-1* or *rap-3,* is found to be expressed in DA neurons and required to maintain the synaptic boundary of DA8 and DA9 motor neurons. Moreover, genetic evidence of my study suggests that *rap-2* acts in Semaphorin-Plexin pathway to regulate synaptic tiling by cycling between GTP- and GDP-bound forms. Furthermore, GTP- and GDP-bound RAP-2 are found to localize at distinct subcellular sites in DA9 synaptic region, providing the evidence that the activities of RAP-2 are spatially regulated hence to modulate synapse dynamic in a spatial manner.

Chapter 4: The Role of the *mig-15* Gene in Synaptic Tiling

4.1 *mig-15* is required for synaptic tiling

mig-15 was identified as the most promising downstream effector of *rap-2,* for two reasons: 1) *mig-15* mutants show obvious synaptic tiling defect; 2) human TNIK, the ortholog of worm MIG-15, has been found to be specifically activated by Rap2A to regulate filamentous actin (F-actin) rearrangement in spreading HEK293 cells (Taira et al., 2004), and in *C. elegans*, branched F-actin was reported to initiate synapse formation (Chia et al., 2014). Mutants of three *mig-15* mutant alleles (*rh80, rh148* and *rh326*) were observed and compared, which show the same level of DA8/DA9 synaptic overlap (Figure 4.1 A, B, C and D). As observed for *plx-1* and *rap-2* mutants, the overlap defect of *mig-15* mutants is also caused by the extension of the DA8 and DA9 synaptic domains (Figure 4.1 E and F). *rh148* hypomorphic allele contains a *V169E* substitution in N-terminal kinase domain; *rh80* and *rh326* alleles contain *W898STOP* in the CNH domain and *Q439STOP* in the intermediate proline-rich domain respectively, hence the above-mentioned observation of *mig-15* mutants suggests that the kinase domain and the citron homology (CNH) domain are both required for the regulation of synaptic tiling. Since *rh148* mutants are healthier than the mutants of the other two alleles, I used *rh148* for all the following experiments.

Furthermore, *mig-15* mutants show more severe synaptic tiling defect than *rap-2* and *plx-1* mutants, indicating that *mig-15* might be involved in multiple signaling pathways to regulate synaptic tiling (see discussion). It has been reported that TNIK

acts at upstream of JNK pathway to regulate cell activities (Becker et al., 2000; Ip and Davis, 1998; Zhu et al., 2005b) , whereas *jnk-1* mutants does not show obvious overlap of DA8 and DA9 synaptic domains (Figure 4.1G and H), indicating that *mig-15* regulates DA9 synapse patterning through other mechanisms.

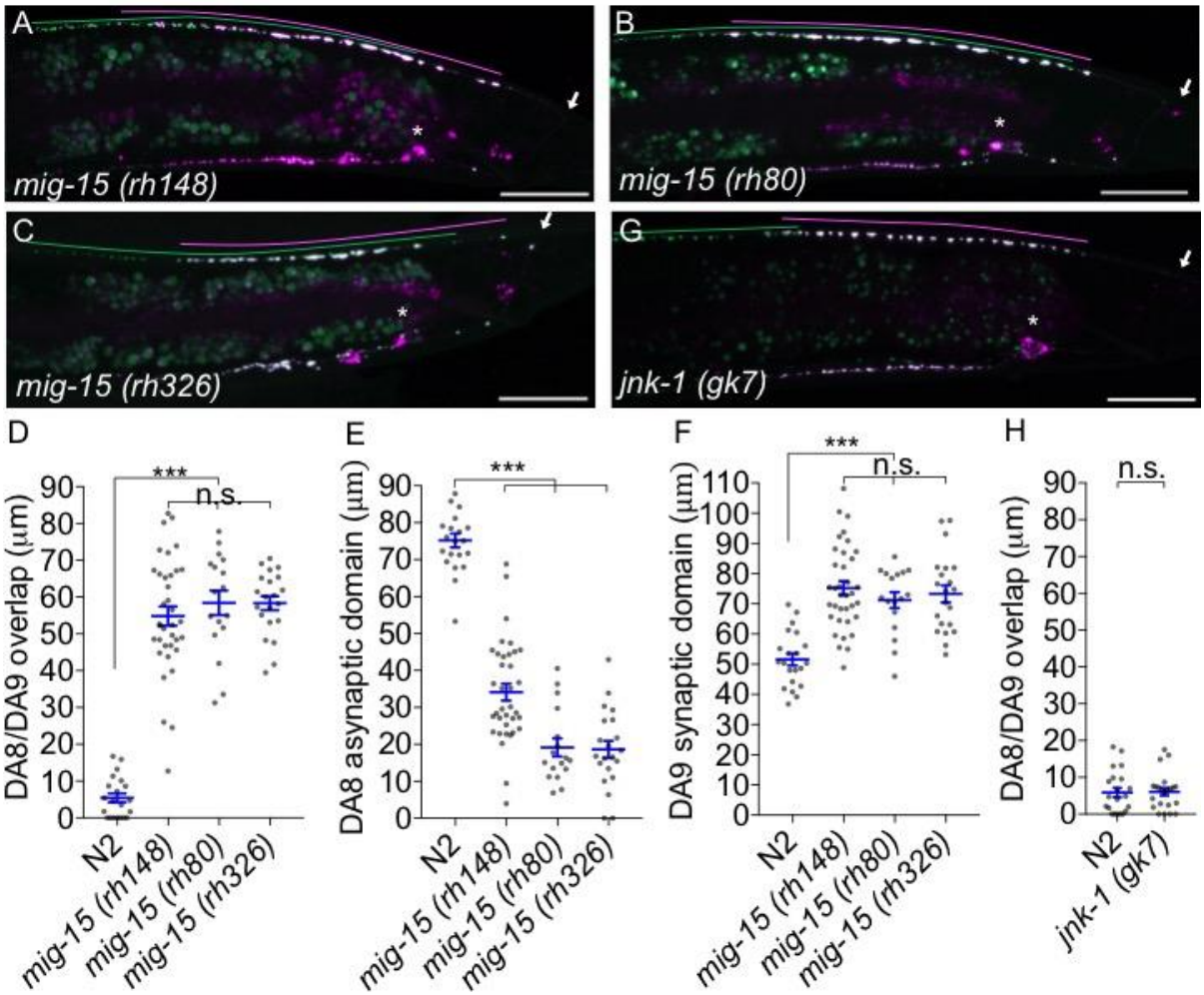

Figure 4.1 *mig-15* is required for synaptic tiling.

(A-C) Synaptic tiling defect of *rh148* (A), *rh80* (B) and *rh326*(C) *mig-15* mutants. (D-F) Quantification of DA8/DA9 overlap (D), DA8 asynaptic domain (E) and DA9 synaptic domain (F) of *mig-15* alleles, each dot represents single animal. (G) Synaptic tiling defect of *jnk-1* mutant. (H) Quantification of DA8/DA9 overlap in *jnk-1* mutants, each dot represents single animal. Error bars represent SEM. ***$p < 0.001$; n.s., not significant (ANOVA/Dunnett for D-F, student t-test for H). Scale bar represents 20 µm. White asterisk and arrow indicate cell body and axon respectively.

4.2 *mig-15* mutants show DA9 axon defect

Previous studies of *mig-15* found that it is required for proper axonal navigation in *C. elegans* (Chapman et al., 2008; Poinat et al., 2002; Shakir et al., 2006). Notably, 42% of *mig-15* mutants displayed axon branching phenotype (Figure 4.2), which is supposed to be accompanied with the deficit of synapse formation (Chia et al., 2014; Gallo, 2011; Meyer and Smith, 2006). 10% of the *mig-15* mutants exhibit DA9 axon guidance defects (Figure 4.2 A-E). These phenotypes indicate that the main function of *mig-15* in DA9 is to regulate synapse formation.

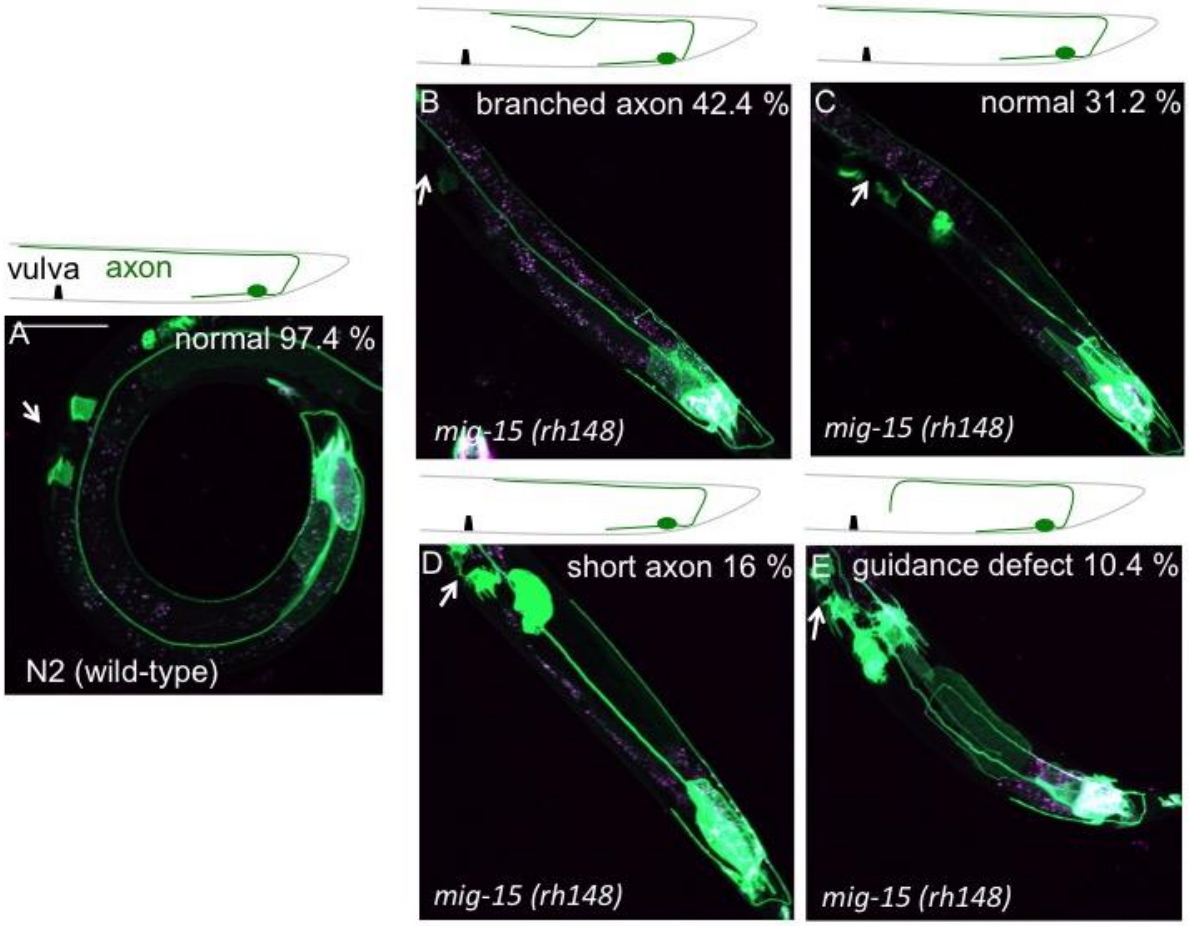

Figure 4.2 DA9 axon defects of *mig-15* mutants.

(A) Representative images and schematic drawings of a DA9 axon in wild-type animal (the DA9 axons of 97.4% animals extend beyond vulva, n=113). (B-E) Representative images of axon defects in *mig-15* mutants. 42.4% of the mutants display branching defects (B), 31.2% of the mutants display wild-type like axon length (C), 16% of the mutants have shorter axons (D) and 10.4% of the mutants show guidance defect (E), 125 animals were observed. Scale bar represents 50 µm for all the images. White arrow denotes vulva.

4.3 mig-15 genetically acts in the same pathway with *rap-2* and *plx-1*

Double mutants were generated to determine if the *plx-1* null (*nc36*), *rap-2* null (*gk11*), *rap-2 G12V* (*miz18*) and *rap-2 S17A* (*miz19*) mutations enhance the DA8/DA9 synaptic overlap of *mig-15* (*rh148*) mutants. As expected, all of the double mutants showed the same level of DA8/DA9 overlap defect as *mig-15* single mutants, supporting the prediction that *mig-15* genetically acts downstream of *plx-1* and *rap-2* pathway (Figure 4.3 A, B, C, D, E and F).

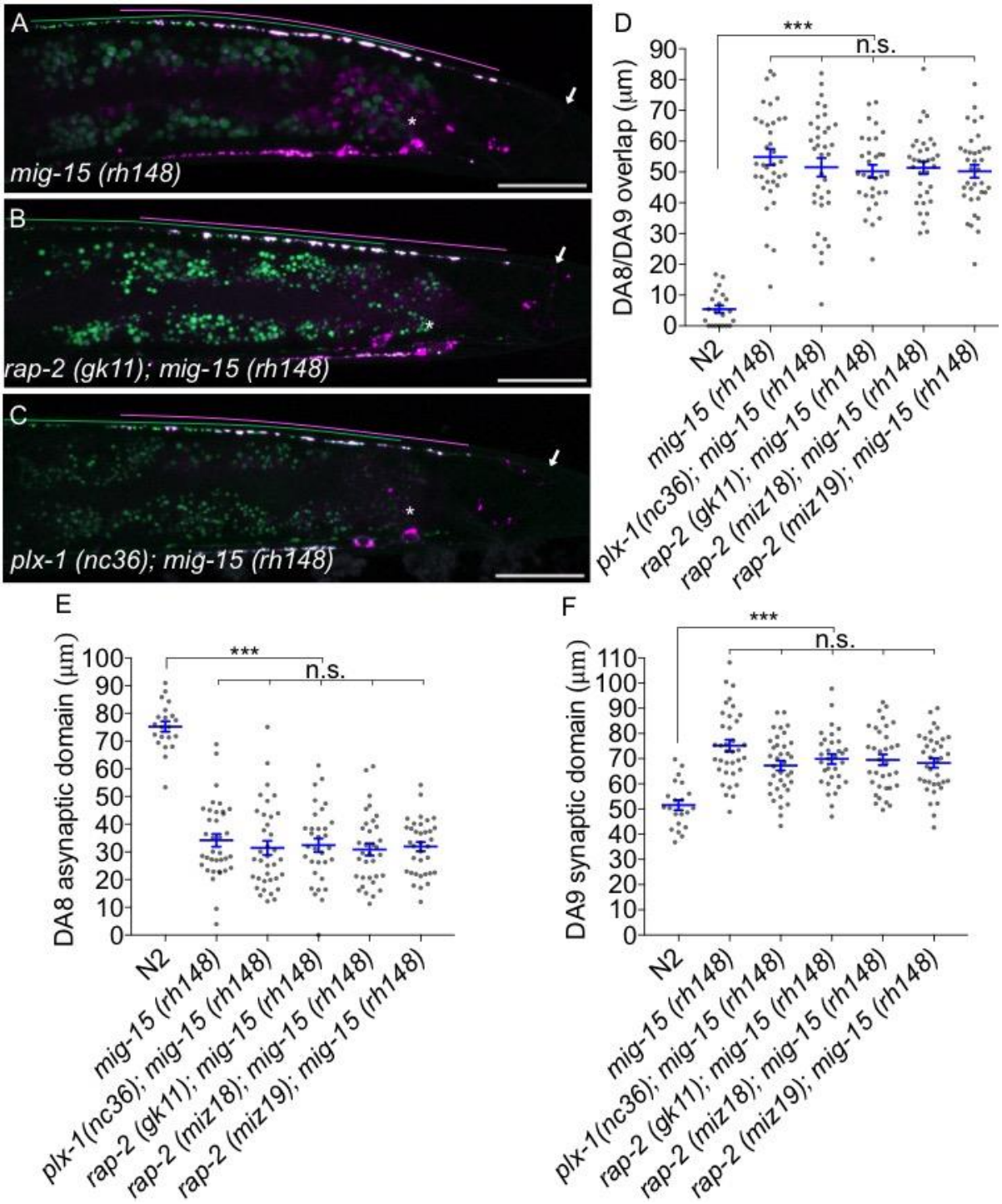
A
mig-15 (rh148)
B
rap-2 (gk11); mig-15 (rh148)
C
plx-1 (nc36); mig-15 (rh148)
D
DA8/DA9 overlap (μm)
***
n.s.
N2
mig-15 (rh148)
plx-1(nc36); mig-15 (rh148)
rap-2 (gk11); mig-15 (rh148)
rap-2 (miz18); mig-15 (rh148)
rap-2 (miz19); mig-15 (rh148)
E
DA8 asynaptic domain (μm)
F
DA9 synaptic domain (μm)

Figure 4.3 ***mig-15* genetically acts in the same pathway with *plx-1* and *rap-2.*** (A-C) Synaptic tiling defect of *mig-15* (A), *plx-1;mig-15* (B) and *rap-2;mig-15* (C) mutants. (D-F) Quantification of DA8/DA9 overlap (D), DA8 asynaptic domain (E) and DA9 synaptic domain (F), each dot represents single animal. Error bars represent SEM; *** $p < 0.001$, n.s., not significant (ANOVA/Tukey). Scale bar represents 20 µm. White asterisk and arrow indicate cell body and axon respectively.

4.4 *mig-15* acts cell autonomously in DA neurons

Previous work of Mizumoto and my study suggest *plx-1* and *rap-2* act cell autonomously in DAs (Mizumoto and Shen, 2013b), I reasoned that *mig-15* also functions in a cell autonomous manner. Since other research groups have found four *mig-15* transcripts (Poinat et al., 2002), the *mig-15* genomic fragment was used to perform cell-specific rescue experiments. As expected, the DAs-specific *mig-15* expression (driven by *unc-4c* promoter) in *mig-15* mutants recovered the tiling pattern of DA8 and DA9 synaptic domains (Figure 4.4 A, F, G and H) (Miller and Niemeyer, 1995). However, the DA9 specific expression (driven by the *mig-13* strong promoter) not only rescued but also strikingly shortened the extended DA9 synaptic domain of *mig-15* mutants (Figure 4.4 B, F, G and H) (Klassen and Shen, 2007); moreover, the expanded DA8 synaptic domain was weakly rescued, indicating the leaky expression of MIG-15 in DA8. This observation was further enforced when the *mig-15* genomic fragment without a promoter weakly rescued DA8/DA9 synaptic overlap (Figure 4.4 F); and the DD class motor neuron-specific expression (driven by *flp-13* promoter) partially recovered the DA8/DA9 tiling pattern (Figure 4.4 C and F) (Shan et al., 2005).

It has been shown that the kinase-dead TNIK acts as dominant-negative mutant and abrogate the transcription of Wnt target genes (Mahmoudi et al., 2009). *mig-15 K50A* kinase-dead mutant (driven by *unc-4c* promoter) grossly induced synaptic tiling defects in wild-type animals (Figure 4.4 D, E, I). Thus, *mig-15* is both necessary and sufficient in DA neurons to regulate synaptic tiling.

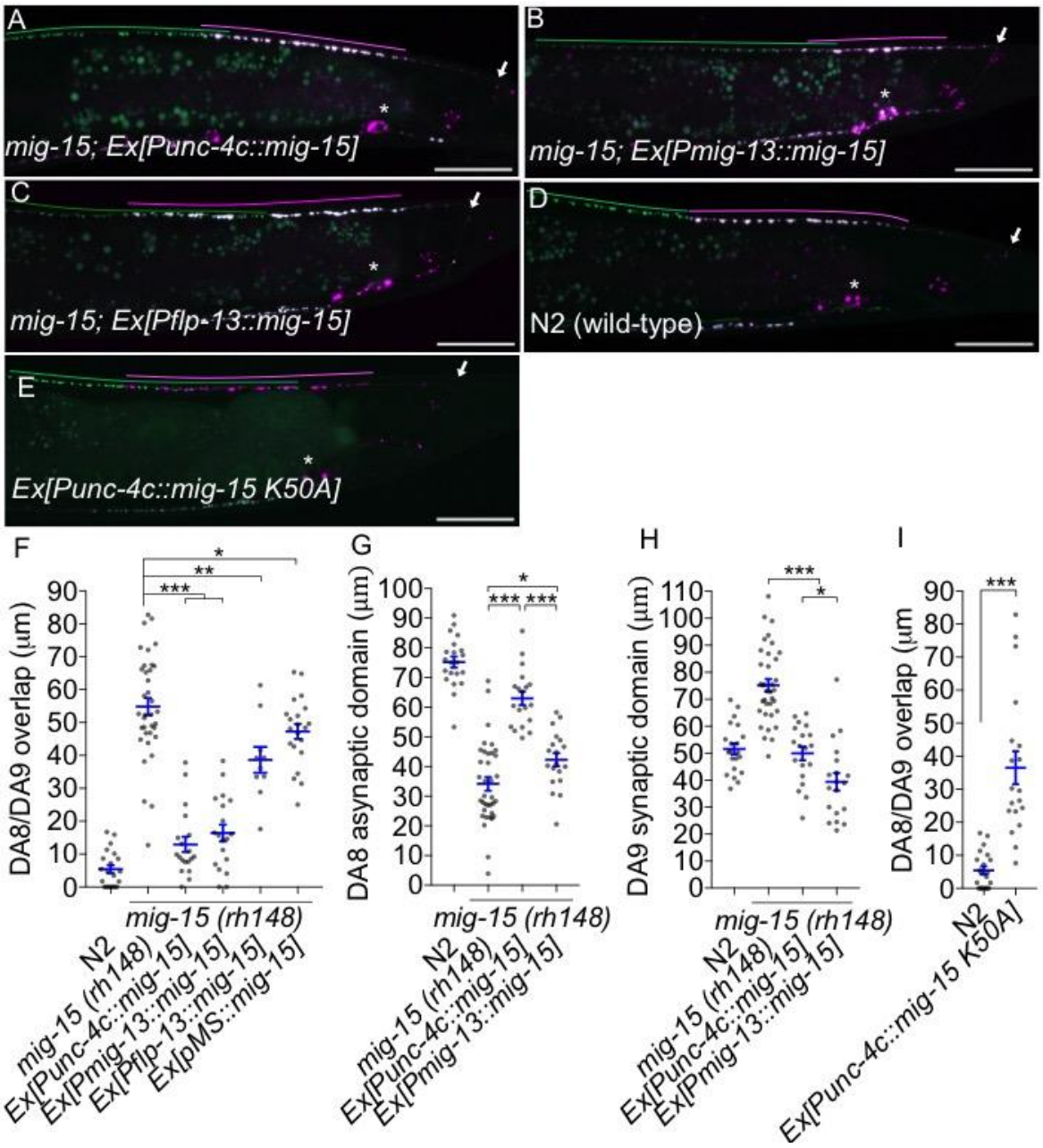

Figure 4.4 *mig-15* acts in DA9 in a cell autonomous manner.

(A-C) Representative images of DAs (A), DA9 (B) and DD (C) rescue in *mig-15* mutants. (D-E) Representatives of wild-type (D) and kinase-dead MIG-15 induced DA8/DA9 synaptic tiling defect in N2 animals (E). (F-H) Quantification of DA8/DA9 overlap (D), DA8 asynaptic domain (G) and DA9 synaptic domain (H) of rescue experiments, each dot represents single animal. (I) Quantification of DA8/DA9 overlap induced by *mig-15 (K50A),* each dot represents single animal. Error bars represent SEM; *** $p < 0.001$, ** $p < 0.01$, * $p < 0.05$ (ANOVA/Tukey for F-H, student t-test for I). Scale bar represents 20 µm. White asterisk and arrow indicate cell body and axon respectively.

4.5 The localization of MIG-15 in DA9

I next sought to detect the localization of MIG-15. I co-expressed the synapse marker mCherry::RAB-3 together with MIG-15::GFP in DA9. The expression of mCherry::RAB-3 was driven by *mig-13* promoter which becomes active in DA9 at an early developmental stage (Klassen and Shen, 2007; Miller and Niemeyer, 1995). The MIG-15::GFP expression was driven by the *itr-1* promoter which becomes active in DA9 after larval 3 stage (L3) (Mizumoto and Shen, 2013b). At L3 mCherry::RAB-3 and diffused MIG-15::GFP were detected across DA9 synaptic region (Figure 4.5 A). However, at L4 stages, I could still detect mCherry::RAB-3 and MIG-15::GFP in the DA9 cell body, punctate MIG-15::GFP and weak mCherry::RAB-3 were observed at the DA9 synaptic domain (Figure 4.5 B), indicating the disappearance of DA9 synapses. As observed in section 4.4, in the *mig-15* mutant background, the expression of *mig-15* (driven by the strong promoter *mig-13)* induced a shorter DA9 synaptic domain and fewer synapses compared to

wild-type animals. These observations suggest that MIG-15 negatively regulates synapse formation, and due to this reason the exact localization of MIG-15 at the synaptic region is hardly detectable once it is overexpressed in DA9.

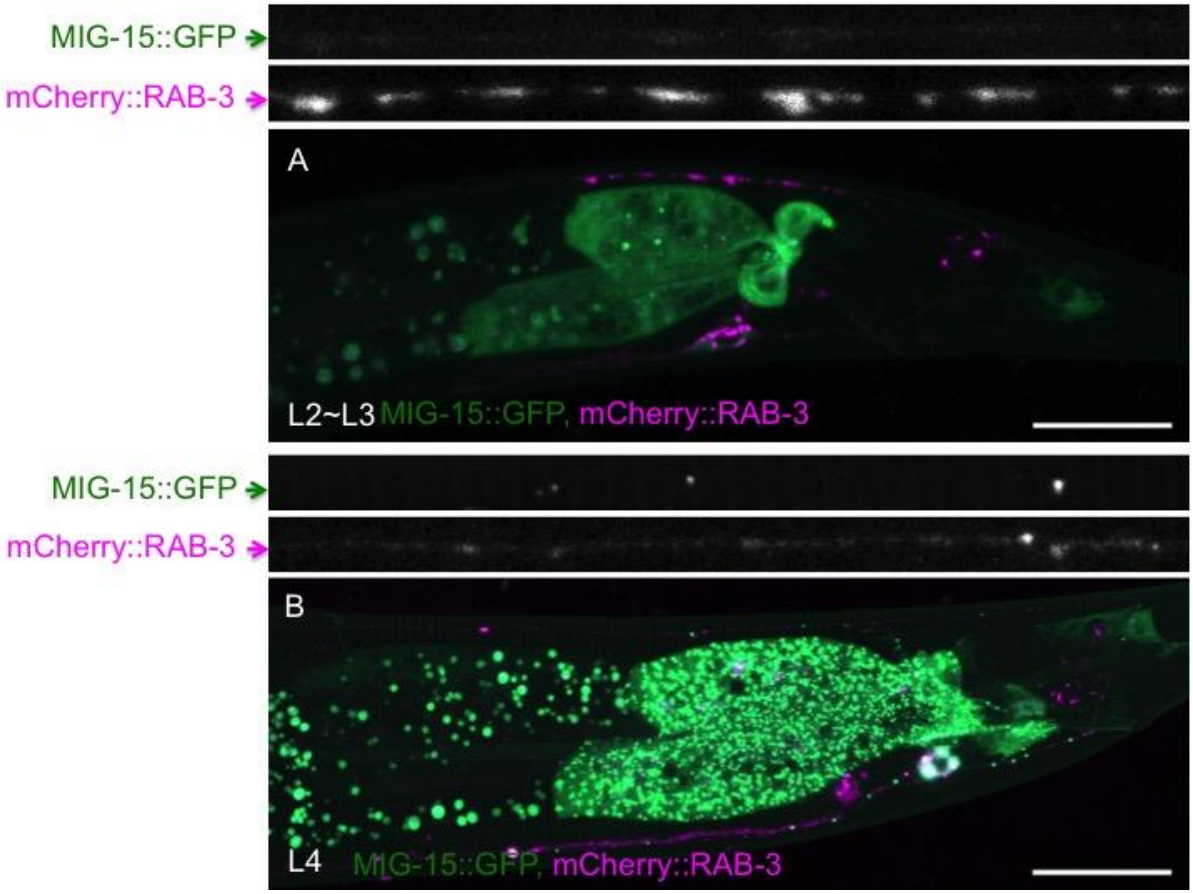

Figure 4.5 Localization of MIG-15.

(A) Representative image of MIG-15 localization at L2~L3 stage, MIG-15::GFP and RAB-3::mCherry at the synaptic domain are magnified on top. (B) Representative image of MIG-15 localization at the L4 stage, MIG-15::GFP and RAB-3::mCherry at the synaptic domain are magnified on top. Scale bar represents 20 µm.

4.6 *mig-15* functions as a negative regulator of DA9 synapse formation

In order to confirm that *mig-15* negatively regulates synapse formation, I performed a series of experiments using a DA9 synaptic marker strain. The number of DA9 synapses was counted in different genetic backgrounds and the length of DA9 synaptic domain from the most posterior to the most anterior DA9 synapse was measured. *mig-15* mutants *(rh148)* significantly show more synapses and longer synaptic domains than N2 animals (Figure 4.6 A, B, D and E), whereas the *mig-15* overexpression (OE) in N2 animals strikingly induced less DA9 synapses and shorter DA9 synaptic domains which do not extend anteriorly as far as in N2 animals (Figure 4.6 C, D and E). MIG-15 (OE) driven by the *flp-13* promoter also induced fewer synapses in DD class motor neurons (Figure 4.6 F and G). Together, these results further demonstrate that *mig-15* functions as a key negative regulator of synapse formation.

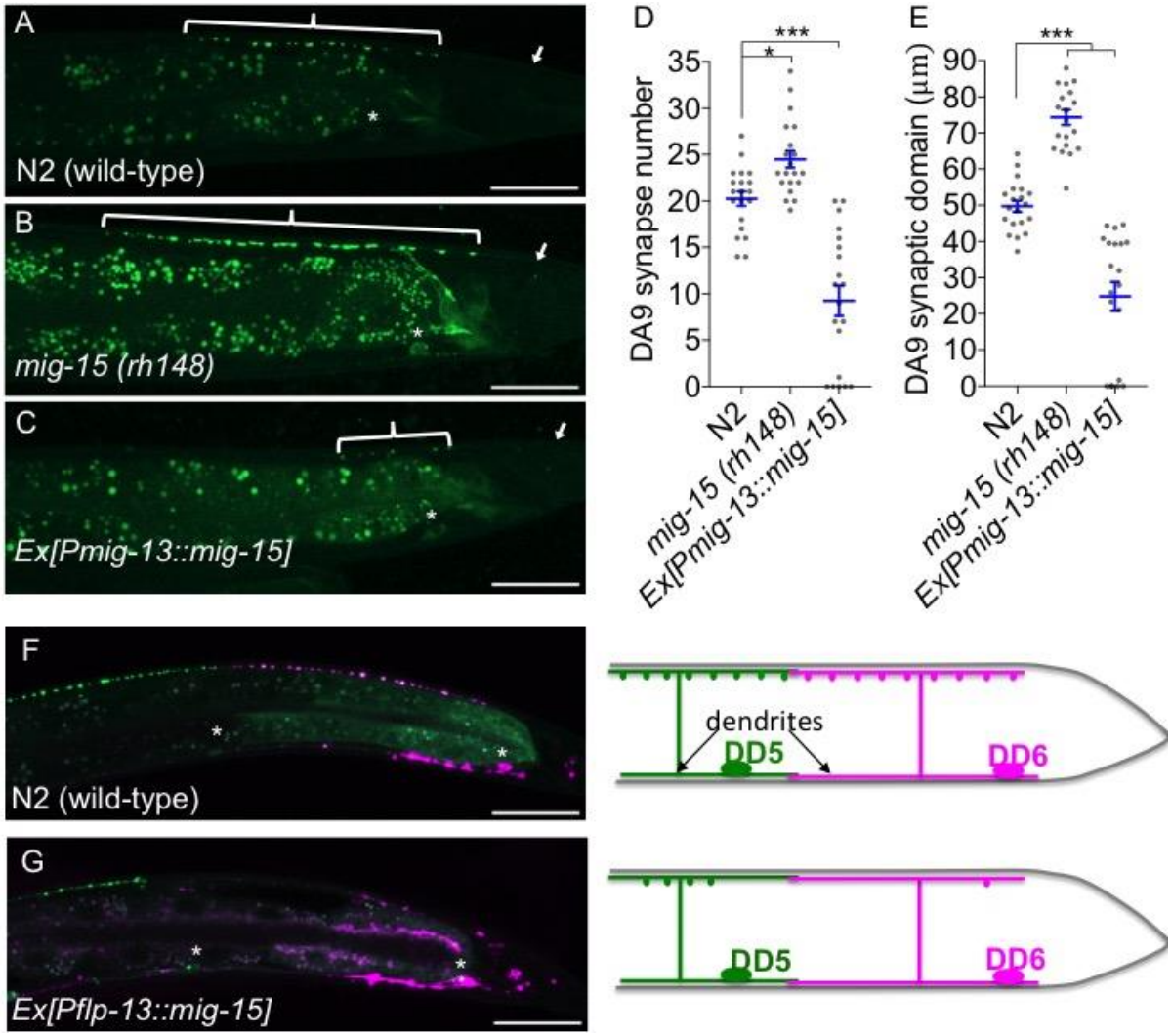

Figure 4.6 ***mig-15* is a negative regulator of synapse formation.**

(A-C) Representative images of the DA9 synaptic domain in wild-type (A), *mig-15* mutant (B) and DA9-MIG-15-overexpressed N2 animal (C), DA9 synaptic domain is bracketed. (D-E) Quantification of the synapse number (D) and the length of DA9 (E), each dot represents single animal. (F-G) DD5/DD6 synaptic domains in wild-type (F) and DDs-MIG-15-overexpressed animal (G), and schematics respectively. Error bars represent SEM; *** $p < 0.001$, * $p < 0.05$, n.s., not significant (ANOVA/Tukey). Scale bars represent 20 µm. White asterisk and arrow indicate the cell body and axon respectively.

4.7 PLX-1/RAP-2 signaling coordinates DA8/DA9 synaptic border

In order to determine the importance of the PLX-1 signaling in synaptic pattern formation, the influence of the MIG-15 (OE) on DA8/DA9 synaptic boundary in wild-type, *plx-1* and *rap-2* mutants backgrounds were observed. In wild-type animals, the DA9 specific MIG-15 (OE) posteriorly shifted the DA8/DA9 synaptic boundary, which is correlated with the posterior extension of the DA8 synaptic domain and posterior shift of the DA9 synaptic border (Figure 4.7 A, D and E). However, despite the reduction of the DA9 synapse number, MIG-15 (OE) did not affect the length of the DA8 and DA9 synaptic domains in *plx-1* and *rap-2* mutants (Figure 4.7 B, C, D and E). Thus, these results suggest that PLX-1/RAP-2 signaling is necessary to coordinate the position of DA8/DA9 boundary.

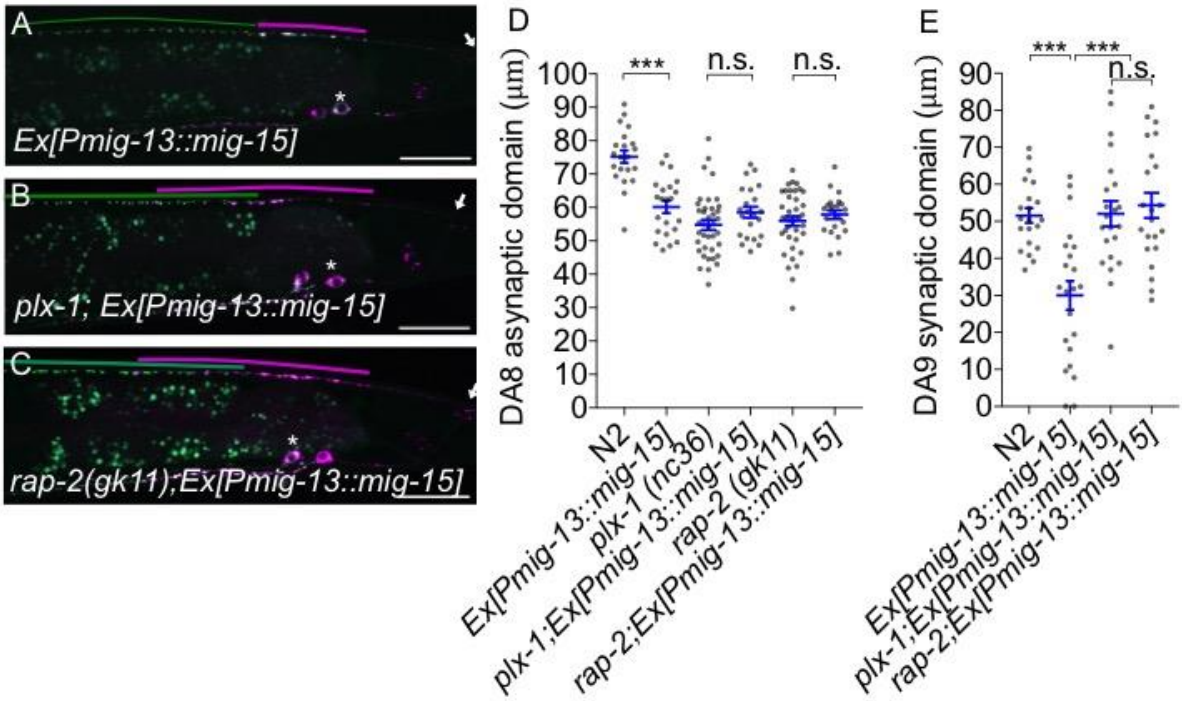

Figure 4.7 PLX-1 signaling adjusts DA8/DA9 synaptic boundary.

(A-C) Representative images of DA8/DA9 synaptic domain in the DA9-MIG-15-overexpressed wild-type animal (A), *plx-1* mutant (B) and *rap-2* mutant (C). (D-E) Quantification of DA8 asynaptic domain (D) and DA9 synaptic domain (E), each dot represents single animal. Error bars represent SEM; *** $p < 0.001$, n.s., not significant (ANOVA/Tukey). Scale bar represents 20 μm. White asterisk and arrow indicate cell body and axon respectively.

4.8 *mig-15* might regulate synapse number via F-actin

TNIK and Rap GTPases were reported to regulate the actin cytoskeleton (Lin et al., 2008, 2010; Taira et al., 2004). It has been shown that branched F-actin initiates synapse formation and is enriched within the DA9 synaptic domain (Chia et al., 2012, 2014; Mizumoto and Shen, 2013b). I reasoned that MIG-15 negatively regulates synapse formation by promoting actin rearrangement. The Utrophin calponin homology domain (Ut-CH) was reported to bind with F-actin (Chia et al., 2014; Galkin et al., 2002), so I used GFP::Ut-CH to visualize F-actin in the DA9 synaptic domain. As expected, *rap-2* and *mig-15* mutants show extended F-actin distribution compared with wild-type animals (Figure 4.8 A, B, C and E). On the contrary, MIG-15 (OE) significantly shortened F-actin distribution in the DA9 synaptic domain (Figure 4.8 D and E). These results support the idea that *mig-15* functions through negatively regulating actin dynamics in the DA9 synaptic domain.

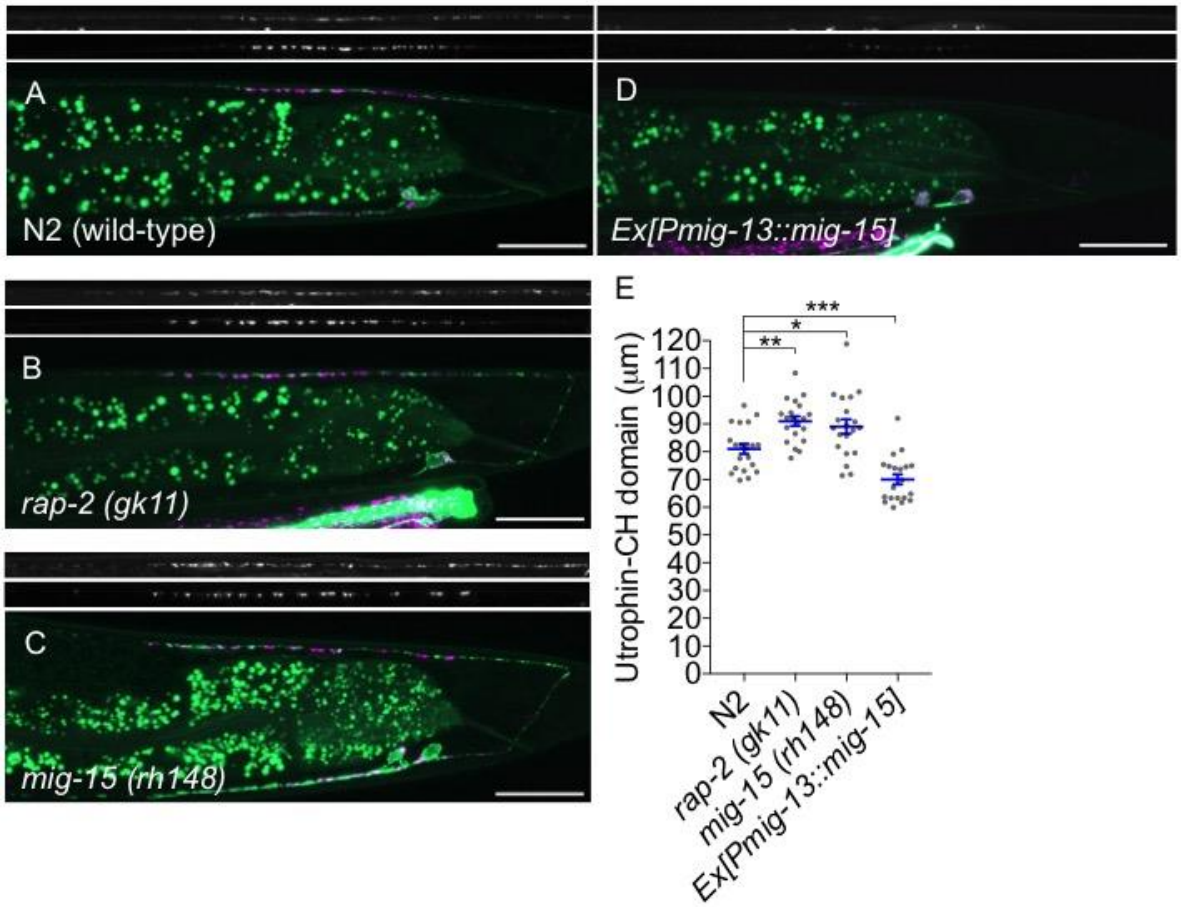

Figure 4.8 ***mig-15* might regulate synapse number via F-actin.**

(A-D) Representative images of the DA9 synaptic domains in wild-type (A), *rap-2* mutant (B) *mig-15* mutant (C) and DA9-MIG-15-overexpressed wild-type animal (D). GFP::Ut-CH and mCherry::RAB-3 are shown separately on top of each panel. (E) Quantification of DA9 synaptic F-actin distribution length, each dot represents single animal. Error bars represent SEM; *** $p < 0.001$, ** $p < 0.01$ and * $p < 0.05$ (ANOVA/Dunnett). Scale bar represents 20 µm.

4.9 Discussion

The fact that the mutants of all three *mig-15* alleles show similar levels of DA8/DA9 synaptic overlap suggests that the N-terminal kinase domain and the CNH domain

are both necessary and important for regulating synaptic tiling. Previous studies showed that TNIK disrupted the cytoskeleton and induced the rounding up of spreading cells (Taira et al., 2004). Moreover, the CNH domain of TNIK and MIG-15 was shown to be the binding site of human Rap2A and worm RAP-2 respectively, and it is required for the TNIK-Rap2A co-localization in cultured HEK293 cells, supporting the importance of the interaction between RAP-2 and MIG-15 in F-actin rearrangement (Taira et al., 2004). Consistent with previous observations by other research groups, in our study, *mig-15* mutants display increased DA9 synapses which is largely related to the dynamics of the F-actin cytoskeleton (Jin and Garner, 2008), indicating a possible function of *mig-15* for the regulation of synapse number.

Notably, *mig-15* mutants show a more severe synaptic tiling defect than *plx-1* and *rap-2* mutants. This suggests that *mig-15* is not only involved in Plexin signaling but also in other pathways that modulate synaptic tiling. Indeed, the CNH domain of MIG-15 was reported to interact with actin activity modulators such as the Rac small GTPases CED-10/RAC1, RAC-2 and MIG-2/RhoG and the cytoplasmic domain of PAT-3, which is a *C. elegans* ortholog of the integrin *β1* subunit (Poinat et al., 2002; Shakir et al., 2006). It is possible that *mig-15* acts as an organizer of multiple pathways involved in actin organization hence it regulates axon and synapse formation.

The fact that *rap-2* mutations do not enhance the phenotype of *mig-15* mutants, combined with the physical interaction (Taira et al., 2004), suggests that RAP-2 and

MIG-15 act together to spatially regulate synaptic tiling. However, the exact mechanism of how the interaction between RAP-2 and MIG-15 regulates F-actin dynamics is unknown. Because both GTP- and GDP-bound Rap2A were observed to interact with TNIK (Taira et al., 2004), it is possible that the spatially regulated RAP-2 changes the conformation of MIG-15 by switching between GTP-binding and GDP-binding configurations, hence regulating the activities of MIG-15. This assumption could also be applied to the spatial distribution of GTP-RAP-2 and GDP-RAP-2 in the DA9 synaptic domain. Once binding with GTP-RAP-2, MIG-15 is inactivated or the active domain is closed, whereas once interacting with GDP-RAP-2 at the peri-synaptic sites, MIG-15 is activated or the active domain is exposed. The exposed active domain then phosphorylates downstream molecules that negatively regulate F-actin dynamics. So that GDP-RAP-2, which is detected to accumulate at the peri-synaptic sites, inhibits synapse formation through activating MIG-15.

Since *mig-15* is the only worm ortholog of vertebrate *MAP4K, MINK* and *TNIK* genes that each has different functions, we do not exclude the possibility that alternative splicing and proteolytic cleavage also contribute to the diverse functions of *mig-15*, which could be regulated by not only Semaphorin-Plexin but also other signal transduction pathways, such as Wnt, Eph and integrin signaling (Becker et al., 2000; Mikryukov and Moss, 2012; Poinat et al., 2002).

4.10 Conclusions

For the study of the *mig-15* gene, I found that *mig-15* mutants show more severe synaptic tiling defects than *plx-1* and *rap-2* mutants, whereas this phenotype is not enhanced by *plx-1* or *rap-2* mutations, suggesting that *mig-15* not only genetically acts downstream of *rap-2* and *plx-1* but also participates in other signaling pathway(s) to regulate synaptic patterning. Furthermore, it is highly possible that MIG-15 functions cell autonomously in DAs to regulate synaptic tiling by physically interacting with RAP-2. As a result, once activated MIG-15 negatively regulates synapse formation by disrupting F-actin hence negatively regulating synapse formation.

Chapter 5: Relationship Study of *plx-1*, *rap-2* and *mig-15*

5.1 *mig-15* requires *plx-1* and *rap-2* to specify DA9 synaptic domain

I next sought to determine the importance of *rap-2* and *plx-1* in the regulation of synapse patterning. For this purpose, MIG-15 was overexpressed in DA9 of both wild-type and *rap-2* and *plx-1* null mutants. The DA9 synaptic domains of twenty animals were aligned into one panel; meanwhile, the synapse number was counted and the length of the DA9 synaptic domain was measured of all the displayed twenty animals from each genotype. Consistent with the observation described in the last chapter, *mig-15* hypomorphic mutants exhibit more synapses and longer synaptic domains (Figure 5.1 A, G, H and I), whereas MIG-15 (OE) in wild-type animals induced fewer synapses and shorter synaptic domains (Figure 5.1 A, B, H and I). However, in *plx-1* and *rap-2* mutants, although the overexpressed MIG-15 also reduced the number of DA9 synapses to the same level as wild-type animals that overexpressing *mig-15* (Figure 5.1 C, D, E, F and I), the length of the DA9 synaptic domain did not become as short as wild-type animals that overexpressing *mig-15* (Figure 5.1 C, D, E, F and H), so that the distribution of DA9 synapses were sparser than *mig-15* overexpressed wild-type animals. These results suggest that *plx-1* and *rap-2* are required to spatially regulate the synapse density.

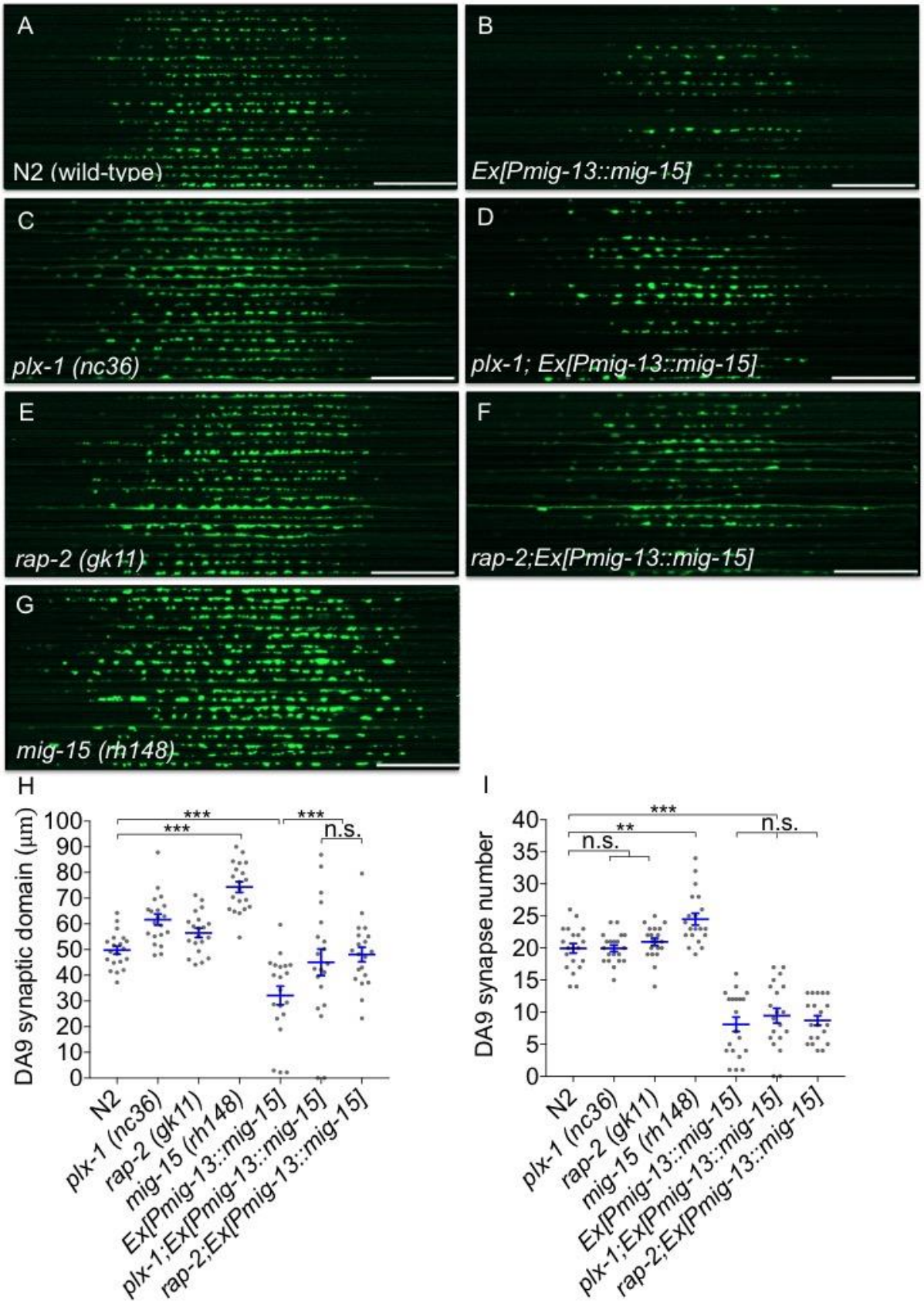
A
N2 (wild-type)
B
Ex[Pmig-13::mig-15]
C
plx-1 (nc36)
D
plx-1; Ex[Pmig-13::mig-15]
E
rap-2 (gk11)
F
rap-2;Ex[Pmig-13::mig-15]
G
mig-15 (rh148)
H
DA9 synaptic domain (μm)
***
***
***
n.s.
N2
plx-1 (nc36)
rap-2 (gk11)
mig-15 (rh148)
Ex[Pmig-13::mig-15]
plx-1;Ex[Pmig-13::mig-15]
rap-2;Ex[Pmig-13::mig-15]
I
DA9 synapse number
***
**
n.s.
n.s.
N2
plx-1 (nc36)
rap-2 (gk11)
mig-15 (rh148)
Ex[Pmig-13::mig-15]
plx-1;Ex[Pmig-13::mig-15]
rap-2;Ex[Pmig-13::mig-15]

Figure 5.1 *mig-15* requires *rap-2* to specify DA9 synaptic domains.

(A-F) Spatial distribution of DA9 synapses in wild-type (A), *plx-1* (C), *rap-2* (E) and *mig-15* (D) mutants and DA9-MIG-15-overexpressed wild-type and *rap-2* mutants. The synaptic domains of 20 animals are aligned in each panel. (G-H) Quantification of DA9 synaptic domains (G) and DA9 synapse number (H). Error bars represent SEM; *** $p < 0.001$, ** $p < 0.01$, n.s., not significant (ANOVA/Tukey). Scale bar represents 20 µm.

5.2 *plx-1* regulates *mig-15* via *rap-2* to specify DA9 synaptic domain

Lastly, I investigated if Semaphorin-Plexin signaling regulates *mig-15* activity via *rap-2*. To test this prediction, I DA9-specifically overexpressed PLX-1 in wild-type, *rap-2 (gk11), mig-15 (rh148)* and *rap-2 (gk11);mig-15 (rh148)* mutants, and compared the phenotype caused by PLX-1 overexpression (OE) among these genotype backgrounds. PLX-1 (OE) did not change the length of DA9 synaptic domain in N2 and *rap-2 (gk11)* animals (Figure 5.2 A, C, F, G). It suppressed extended DA9 synaptic domain of *mig-15 (rh148)* mutants (Figure 5.2 B, F, G). However, quantification of these results suggest PLX-1 (OE) has no suppression in the *rap-2 (gk11);mig-15 (rh148)* double mutant background (Figure 5.2 D, E, F, G). Because *mig-15(rh148)* is a hypomorphic allele which still produces partially functional MIG-15 kinase (Chapman et al., 2008), our results suggest that in the mutants which only carry the *rh148* mutation, PLX-1 (OE) recovered MIG-15 activity to some extent, but in the absence of the *rap-2* gene, PLX-1 (OE) was not able to rescue the MIG-15 hypomorph. Together, these results indicate that PLX-1 specifies synaptic patterning via RAP-2 GTPase and MIG-15 kinase.

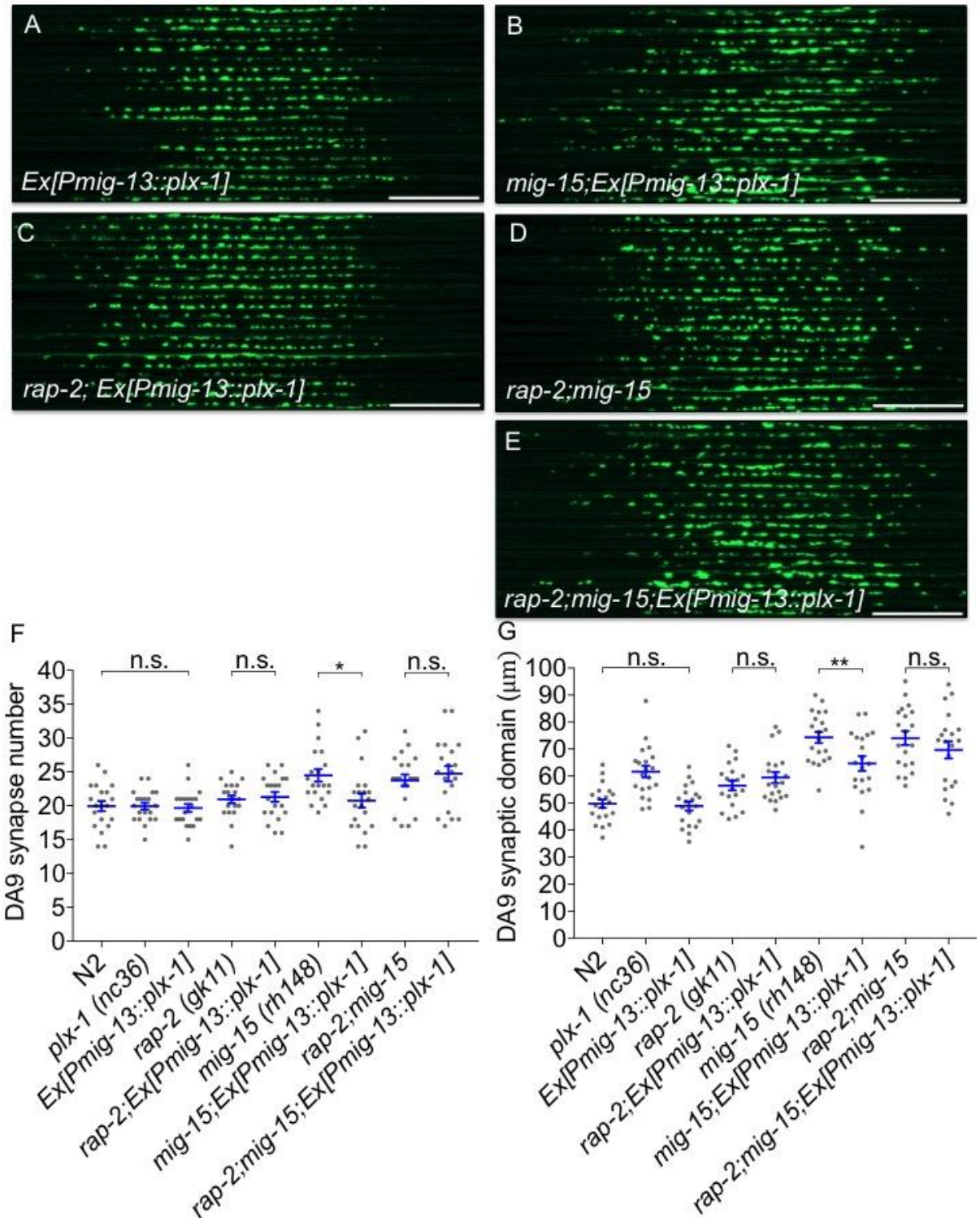
A
Ex[Pmig-13::plx-1]
B
mig-15;Ex[Pmig-13::plx-1]
C
rap-2; Ex[Pmig-13::plx-1]
D
rap-2;mig-15
E
rap-2;mig-15;Ex[Pmig-13::plx-1]
F
DA9 synapse number
n.s.
n.s.
*
n.s.
N2
plx-1 (nc36)
Ex[Pmig-13::plx-1]
rap-2 (gk11)
rap-2;Ex[Pmig-13::plx-1]
mig-15 (rh148)
mig-15;Ex[Pmig-13::plx-1]
rap-2;mig-15
rap-2;mig-15;Ex[Pmig-13::plx-1]
G
DA9 synaptic domain (µm)
n.s.
n.s.
**
n.s.

Figure 5.2 ***plx-1* regulates *mig-15* via *rap-2* to specify DA9 synaptic domains.** (A-E) Spatial distribution of DA9 synapses in the *rap-2;mig-15* mutants (D) and DA9-PLX-1-overexpressed wild-type (A), *mig-15* (B), *rap-2* (C) and *rap-2;mig-15 (E)*. The synaptic domains of 20 animals are aligned in each panel. (F-G) Quantification of DA9 synapse numbers (F) and length of DA9 synaptic domains (G), each dot represents single animal. Error bars represent SEM; ** $p < 0.01$, * $P < 0.05$, n.s., not significant (ANOVA/Tukey). Scale bar represents 20 µm.

5.3 Discussion

Synaptogenesis and synapse elimination are both important to form, refine and specify the synaptic connectivity during synaptic pattern formation (Kawabe and Brose, 2011). They were reported to be dynamically regulated throughout the lifespan of an organism and of big importance for learning, memory, behavior and adaptation. For instance, DD class motor neurons of *C. elegans* initially innervate ventral muscle during embryogenesis and the early larvae one stage, whereas from late larvae one stage the ventral synapses will be eliminated and rewire on the dorsal muscle (Kurup and Jin, 2016; White et al., 1978). In the mammalian brain, up to 50% of initially generated synapses will be eliminated during late brain development (Huttenlocher et al., 1982; Zecevic and Rakic, 1991). Numbers of repulsive ligand-receptor recognitions were found to negatively regulate synapse formation, but their underlying molecular mechanisms are poorly understood.

Semaphorin-Plexin signaling was recently found not only to function as an axonal guidance cue but also regulate synapse specificity. In mice, Sema3e and Plxnd1

were reported to be selectively expressed in proprioceptive sensory and motor neurons respectively and function as repellent signaling to restrict synapse formation hence to realize the specificity of sensory-motor monosynaptic connection (Pecho-Vrieseling et al., 2009). In *C. elegans*, this signaling was found to function repulsively to specify the synaptic border between DA class motor neurons in an autocrine manner. However, the molecular mechanism and intracellular components of this signaling are still poorly understood and unidentified (Mizumoto and Shen, 2013b; Pecho-Vrieseling et al., 2009). In this study, I demonstrated that in *C. elegans* Semaphorin-Plexin signaling specifies the synaptic border of DA9 by negatively regulating synapse formation via RAP-2 and MIG-15. To the best of my knowledge, this is the first time that RAP-2 and MIG-15 are shown to be involved in Semaphorin-Plexin signaling.

In this chapter, in order to further investigate and support the relationship among PLX-1, RAP-2 and MIG-15, I performed a series of overexpression experiments. First, I compared how MIG-15 overexpression changes the synaptic patterning of DA9 neuron in wild-type animals and *rap-2* mutants animals. The results clearly suggested that RAP-2 is important for maintaining synapse density, and this is possible because the cycle of RAP-2 between GTP- and GDP-bound forms guide the spatial activity of MIG-15 to regulate synapse formation. These results are consistent with the previous findings of small GTPases, that is, the compartmentalized small GTPases interact with their specific downstream effectors to regulate cell activity at a subcellular level (Takai et al., 2001). Furthermore, the

subcellular activities of small GTPases are largely dependent on the distribution of their upstream regulators GAPs and GEFs. Second, by overexpressing PLX-1 in DA9, I further showed that the synaptic border that accumulated PLX-1 inhibits the overextension of the DA9 synaptic domain by activating the negative synapse regulator MIG-15. Together, these results strongly suggest that Semaphorin-Plexin signaling specifies the synaptic patterning of DA neurons via RAP-2 and MIG-15.

Lastly, the novel Semaphorin-Plexin-Rap2-TNIK pathway identified by this work is not the sole cascade in the regulation of the synaptic pattern formation. Since the cytoplasmic part of PLX-1 contains multiple interesting domains, it is possible that PLX-1 not only regulates RAP-2 but also interacts with other molecules to restrict the DA9 synaptic border. For instance, Plexin contains a Rho small GTPase binding domain that was found to physically interact with Rac1, RND and RhoD; so far the cytoplasmic region of Plexin has been found to interact with more than 20 proteins (Gay et al., 2011; Hota and Buck, 2012; Pascoe et al., 2015b). Rap2 was also found to interact with a number of proteins, such as Ral GEFs (RalGDS, Raf, PI3K) and RhoGAP (PARG1), so it is possible that RAP-2 associates with multiple effectors to regulate synaptic tiling (Myagmar et al., 2005; Nancy et al., 1999). Finally, as discussed in chapter 4, due to the severe synaptic tiling defect displayed by *mig-15* mutants, besides the Semaphorin-Plexin pathway, MIG-15 seems to be involved in other signaling pathways as well (such as Wnt, Netrin, and Integrin) and functions as a key organizer of the signaling networks to regulate synapse formation (Becker et al., 2000; Mizumoto and Shen, 2013a; Poinat et al., 2002; Yang et al., 2014). Future

work is needed to clarify and sort out the complex mechanisms underlying synaptic tiling.

5.4 Conclusions

For the study of this chapter, MIG-15 was first found to negatively regulate synapse formation, and RAP-2 functions spatially to control the synapse density across the DA9 synaptic domain. Further study of this section supported that RAP-2 indeed mediates the extracellular Semaphorin-Plexin signal to the intracellular effector MIG-15, hence specifying the synaptic patterning of DA9 neuron.

Chapter 6: The Model of DA8/DA9 Synaptic Tiling and Future Directions

6.1 The model of the DA8/DA9 synaptic tiling

Mizumoto has demonstrated that the DA8/DA9 synaptic tiling is dependent on the interaction between the DA8 and DA9 axons on the dorsal nerve cord (Mizumoto and Shen, 2013b). Based on the DA8/DA9 axonal interaction, a model was proposed to illustrate how PLX-1 (concentrated at the DA9 synaptic border as shown in Figures 1.3 and 6.1) and the unknown signaling molecule(s) (localized at the DA8 asynaptic border as shown in Figure 6.1) mutually inhibit each other's distribution to specify the DA8/DA9 synaptic boundary, therefore maintaining the DA8/DA9 synaptic tiling.

PLX-1 enriches at the frontier of DA9 synaptic domain and functions autonomously in the DA9 neuron to inhibit the formation of DA9 synapses; meanwhile, the unknown signaling molecule(s) functions in DA8 asynaptic domain to inhibit the DA8 synapse formation (Mizumoto and Shen, 2013b). In this study, *mig-15* and *rap-2* are found to act in not only DA9 but also other DA neurons to maintain DA8/DA9 synaptic tiling (see Figures 3.5 and 4.4). Moreover, 1) GTP- and GDP-bound RAP-2 are localized at distinct subcellular sites and both are needed for maintaining synaptic tiling (see Figures 3.7 and 3.8), indicating the cycling of RAP-2 is spatially regulated and GTP- and GDP-bound RAP-2 both play a role in synaptic patterning; 2) MIG-15 is a key negative regulator of synapse formation and PLX-1 is accumulated at the DA9 synaptic border to increases the concentration of local

GDP-bound RAP-2 which activates MIG-15, therefore inhibiting synapse formation (see Figures 4.6, 4.7 and 5.2).

Based on the above-mentioned findings and inferences, the previous model proposed by Mizumoto is further supported and optimized by adding RAP-2 and MIG-15 into it: SEMA/PLX-1 signaling regulates the activities of RAP-2 and MIG-15 to inhibit the synapse formation at the DA9 synaptic border; and the unknown signaling molecule(s) in DA8 inhibits synapse formation at DA8 asynaptic border also through regulating the activities of RAP-2 and MIG-15, either directly or indirectly (see Figure 6.1, indicated by dotted arrow in DA8).

The present study not only identifies *rap-2* and *mig-15* to address the intracellular mechanism of SEMA/PLX-1 signaling that functions in the DA9 neuron, but also provides the evidence that *rap-2* and *mig-15* are also involved in the inhibitory mechanism of DA8 synapse formation. Because *mig-15* (OE) was found to induce the reduction of DA9 synapses, which is correlated with less DA9 synaptic F-actin, it is possible that GDP-bound RAP-2 and MIG-15 inhibit synapse formation in both DA8 and DA9 by regulating actin dynamics through an unidentified mechanism (see Figure 6.1, indicated by arrows between “F-actin” and “Synapse formation” in DA8 and DA9).

In order to address DA8/DA9 synaptic patterning, it is necessary to systematically expound how is synapse formation cooperatively regulated by repulsive and

attractive mechanisms. More components involved in these processes need to be identified and studied: 1) the unknown molecule(s) from DA8 that impact the distribution of PLX-1 at DA9 synaptic border; 2) the relation between this unknown molecule and the formation of GDP-bound RAP-2 in DA8 (Figure 6.1, indicated by a dotted arrow in DA8 between “Unknown” and the bent arrow); 3) the molecules that cooperate with GTP-bound RAP-2 in the regulation of synaptic patterning, such as the GEFs or downstream effectors of GTP-bound RAP-2, and how they are related to synapse formation; 4) because TNIK was found to induce F-actin rearrangement, I speculated that in worms MIG-15 functions as an actin reorganizer to negatively regulate synapse formation, however, further evidence is needed to clarify how actin network is disrupted by overexpressed MIG-15 in DA9 pre-synapses.

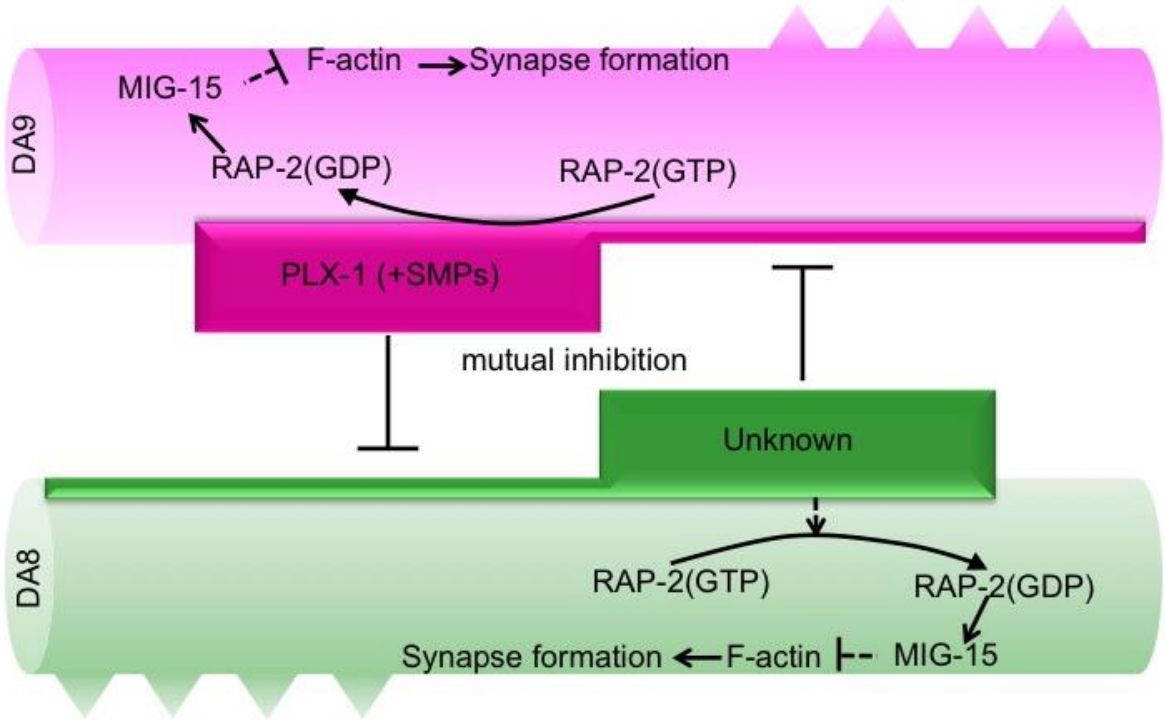

Figure 6.1 The Model of the DA8/DA9 synaptic tiling.

Magenta column and triangles represent DA9 axon and synapses respectively; green column and triangles represent DA8 axon and synapses respectively. Extracellularly, PLX-1 and the unknown molecule mutually inhibit each other's distribution in DA9 and DA8 synaptic border respectively; intracellularly, PLX-1 and the unknown molecule respectively regulate the activity of RAP-2/MIG-15 in DA8 and DA9 to inhibit synapse formation. Arrow indicates activation, flat arrow indicates inhibition, and dotted arrow indicates unidentified signaling.

6.2 Future directions

By studying synaptic tiling we identified two novel components of the Semaphorin-Plexin pathway, but there are still many questions remaining to be answered.

First, since I proposed that PLX-1 accumulates at the border of DA9 synaptic domain to restrict synapse formation, whereas in *sema* mutants PLX-1 localization is completely disrupted, it will be interesting to know if PLX-1 localization is also affected in *rap-2* and *mig-15* mutants, if so, how and why is it disrupted. Recently, in vitro analysis illustrated that myosin VI is responsible for transporting PlexinD1 to subcellular sites (Shang et al., 2017). We are interested to find out if the actin network is disrupted in *mig-15* mutants, and how localization of PLX-1 would be influenced.

Second, Rap2 and TNIK/MIG-15 are known to regulate many cell activities and be involved in multiple signaling pathways. It is, therefore, of great interest to identify

the effectors and components of the Rap2-TNIK complex. One of our findings is that *jnk-1* mutants do not show synaptic tiling defects, suggesting that the activation of the JNK-1 pathway might not participate in synaptic tiling regulation. One of our future directions will be focusing on searching for other components of the Semaphorin-Plexin-Rap2-TNIK pathway.

Finally, why do *mig-15* mutants show more severe synaptic tiling defects than *plx-1* and *rap-2* mutants? What are the other signaling pathways that responsible for the complexity of the synaptic pattern formation of DA neurons? To answer these questions, it will be of great importance to investigate other genes that regulate the activities of *rap-2* and *mig-15,* especially the unknown gene(s) that functions in DA8 to inhibit the DA8/DA9 synapse formation. What we are trying to illustrate in synapse pattern formation is not limited to neuronal development, but also providing insights for physiology and pathology research, such as immune response and cancer.

Bibliography

Alto, L.T., and Terman, J.R. (2017). Semaphorins and their Signaling Mechanisms. Methods Mol. Biol. Clifton NJ *1493*, 1–25.

Ango, F., di Cristo, G., Higashiyama, H., Bennett, V., Wu, P., and Huang, Z.J. (2004). Ankyrin-based subcellular gradient of neurofascin, an immunoglobulin family protein, directs GABAergic innervation at purkinje axon initial segment. Cell *119*, 257–272.

Arribere, J.A., Bell, R.T., Fu, B.X.H., Artiles, K.L., Hartman, P.S., and Fire, A.Z. (2014). Efficient Marker-Free Recovery of Custom Genetic Modifications with CRISPR/Cas9 in Caenorhabditis elegans. Genetics *198*, 837–846.

Becker, E., Huynh-Do, U., Holland, S., Pawson, T., Daniel, T.O., and Skolnik, E.Y. (2000). Nck-interacting Ste20 kinase couples Eph receptors to c-Jun N-terminal kinase and integrin activation. Mol. Cell. Biol. *20*, 1537–1545.

Berkel, W.P., Verheijen, M.H.G., Cuppen, E., Asahina, M., Rooij, J. de, Jansen, G., Plasterk, R.H.A., Bos, J.L., and Zwartkruis, F.J.T. (2005). Requirement of the Caenorhabditis elegans RapGEF pxf-1 and rap-1 for Epithelial Integrity. Mol. Biol. Cell *16*, 106–116.

Bos, J.L., Rehmann, H., and Wittinghofer, A. (2007). GEFs and GAPs: Critical Elements in the Control of Small G Proteins. Cell *129*, 865–877.

Braitenberg (1967). Patterns of projection in the visual system of the fly. I. Retina-lamina projections. ExpBrain Res 271–298.

Brenner, S. (1974). The genetics of Caenorhabditis elegans. Genetics *77*, 71–94.

Buck, L.B. (1996). Information coding in the vertebrate olfactory system. Annu. Rev. Neurosci. *19*, 517–544.

Buday, L., and Downward, J. (2008). Many faces of Ras activation. Biochim. Biophys. Acta BBA - Rev. Cancer *1786*, 178–187.

Chapman, J.O., Li, H., and Lundquist, E.A. (2008). The MIG-15 NIK kinase acts cell-autonomously in neuroblast polarization and migration in C. elegans. Dev. Biol. *324*, 245–257.

Chia, P.H., Patel, M.R., and Shen, K. (2012). NAB-1 instructs synapse assembly by linking adhesion molecules and F-actin to active zone proteins. Nat. Neurosci. *15*, 234–242.

Chia, P.H., Chen, B., Li, P., Rosen, M.K., and Shen, K. (2014). Local F-actin Network Links Synapse Formation and Axon Branching. Cell *156*, 208–220.

Clandinin, T.R., and Zipursky, S.L. (2002). Making Connections in the Fly Visual System. Neuron *35*, 827–841.

Di, J., Huang, H., Wang, Y., Qu, D., Tang, J., Cheng, Q., Lu, Z., Zhang, Y., and Zheng, J. (2015). p53 target gene Rap2B regulates the cytoskeleton and inhibits cell spreading. J. Cancer Res. Clin. Oncol. *141*, 1791–1798.

Dickinson, D.J., Ward, J.D., Reiner, D.J., and Goldstein, B. (2013). Engineering the Caenorhabditis elegans genome using Cas9-triggered homologous recombination. Nat. Methods *10*, 1028–1034.

Ding, J.B., Oh, W.-J., Sabatini, B.L., and Gu, C. (2012). Semaphorin 3E-Plexin-D1 signaling controls pathway-specific synapse formation in the striatum. Nat. Neurosci. *15*, 215–223.

Friedland, A.E., Tzur, Y.B., Esvelt, K.M., Colaiácovo, M.P., Church, G.M., and Calarco, J.A. (2013). Heritable genome editing in C. elegans via a CRISPR-Cas9 system. Nat. Methods *10*, 741–743.

Frische, E.W., Berkel, W.P., Haaften, G. van, Cuppen, E., Plasterk, R.H., Tijsterman, M., Bos, J.L., and Zwartkruis, F.J.T. (2007a). RAP‐1 and the RAL‐1/exocyst pathway coordinate hypodermal cell organization in *Caenorhabditis elegans*. EMBO J. *26*, 5083–5092.

Frische, E.W., Berkel, W.P., Haaften, G. van, Cuppen, E., Plasterk, R.H., Tijsterman, M., Bos, J.L., and Zwartkruis, F.J.T. (2007b). RAP‐1 and the RAL‐1/exocyst pathway coordinate hypodermal cell organization in Caenorhabditis elegans. EMBO J. *26*, 5083–5092.

Fu, C.A., Shen, M., Huang, B.C.B., Lasaga, J., Payan, D.G., and Luo, Y. (1999). TNIK, a Novel Member of the Germinal Center Kinase Family That Activates the c-Jun N-terminal Kinase Pathway and Regulates the Cytoskeleton. J. Biol. Chem. *274*, 30729–30737.

Fu, Z., Lee, S.H., Simonetta, A., Hansen, J., Sheng, M., and Pak, D.T.S. (2007). Differential roles of Rap1 and Rap2 small GTPases in neurite retraction and synapse elimination in hippocampal spiny neurons. J. Neurochem. *100*, 118–131.

Fujii, T., Nakao, F., Shibata, Y., Shioi, G., Kodama, E., Fujisawa, H., and Takagi, S. (2002). Caenorhabditis elegans PlexinA, PLX-1, interacts with transmembrane semaphorins and regulates epidermal morphogenesis. Development *129*, 2053–2063.

Galkin, V.E., Orlova, A., VanLoock, M.S., Rybakova, I.N., Ervasti, J.M., and Egelman, E.H. (2002). The utrophin actin-binding domain binds F-actin in two different modes: implications for the spectrin superfamily of proteins. J. Cell Biol. *157*, 243–251.

Gallo, G. (2011). The cytoskeletal and signaling mechanisms of axon collateral branching. Dev. Neurobiol. *71*, 201–220.

Gay, C.M., Zygmunt, T., and Torres-Vázquez, J. (2011). Diverse functions for the semaphorin receptor PlexinD1 in development and disease. Dev. Biol. *349*, 1–19.

Goh, G.Y.S., Martelli, K.L., Parhar, K.S., Kwong, A.W.L., Wong, M.A., Mah, A., Hou, N.S., and Taubert, S. (2014). The conserved Mediator subunit MDT-15 is required for oxidative stress responses in Caenorhabditis elegans. Aging Cell *13*, 70–79.

Guo, X.-X., An, S., Yang, Y., Liu, Y., Hao, Q., and Xu, T.-R. (2016). Rap-Interacting Proteins are Key Players in the Rap Symphony Orchestra. Cell. Physiol. Biochem. *39*, 137–156.

Hall, A. (1990). The Cellular Functions of Small GTP-Binding Proteins. Sci. Wash. *249*, 635.

Hall, A. (1992). Ras-related GTPases and the cytoskeleton. Mol. Biol. Cell *3*, 475–479.

Hayashi, M., Nakashima, T., Taniguchi, M., Kodama, T., Kumanogoh, A., and Takayanagi, H. (2012). Osteoprotection by semaphorin 3A. Nature *485*, 69–74.

Hota, P.K., and Buck, M. (2012). Plexin structures are coming: opportunities for multilevel investigations of semaphorin guidance receptors, their cell signaling mechanisms, and functions. Cell. Mol. Life Sci. CMLS *69*, 3765–3805.

Huttenlocher, P.R., de Courten, C., Garey, L.J., and Van der Loos, H. (1982). Synaptogenesis in human visual cortex--evidence for synapse elimination during normal development. Neurosci. Lett. *33*, 247–252.

Ip, Y.T., and Davis, R.J. (1998). Signal transduction by the c-Jun N-terminal kinase (JNK) — from inflammation to development. Curr. Opin. Cell Biol. *10*, 205–219.

Jin, Y., and Garner, C.C. (2008). Molecular Mechanisms of Presynaptic Differentiation. Annu. Rev. Cell Dev. Biol. *24*, 237–262.

Kawabe, H., and Brose, N. (2011). The role of ubiquitylation in nerve cell development. Nat. Rev. Neurosci. *12*, 251–268.

Ken Matsumoto, Takuya Asano, and Takeshi Endo (1997). Novel small GTPase M-Ras participates in reorganization of actin cytoskeleton. Publ. Online 11 Novemb. 1997 Doi101038sjonc1201416 *15*.

Kielland, A., Bochorishvili, G., Corson, J., Zhang, L., Rosin, D.L., Heggelund, P., and Zhu, J.J. (2009). Activity Patterns Govern Synapse-Specific AMPA Receptor Trafficking between Deliverable and Synaptic Pools. Neuron *62*, 84–101.

Kim, H., Ishidate, T., Ghanta, K.S., Seth, M., Conte, D., Shirayama, M., and Mello, C.C. (2014). A Co-CRISPR Strategy for Efficient Genome Editing in Caenorhabditis elegans. Genetics *197*, 1069–1080.

Kirshfeld (1967). Die Projecktion frt optischen Umwelt auf das Raster der Rhabdomere im Komplexauge von Musca. Exp Brain Res.

Klassen, M.P., and Shen, K. (2007). Wnt signaling positions neuromuscular connectivity by inhibiting synapse formation in C. elegans. Cell *130*, 704–716.

Klassen, M.P., Wu, Y.E., Maeder, C.I., Nakae, I., Cueva, J.G., Lehrman, E.K., Tada, M., Gengyo-Ando, K., Wang, G.J., Goodman, M., et al. (2010). An Arf-like small G protein, ARL-8, promotes the axonal transport of presynaptic cargoes by suppressing vesicle aggregation. Neuron *66*, 710–723.

Kolodkin, A.L., Matthes, D.J., and Goodman, C.S. (1993). The semaphorin genes encode a family of transmembrane and secreted growth cone guidance molecules. Cell *75*, 1389–1399.

Krause, M., Fire, A., Harrison, S.W., Priess, J., and Weintraub, H. (1990). CeMyoD accumulation defines the body wall muscle cell fate during C. elegans embryogenesis. Cell *63*, 907–919.

Kumanogoh, A., Shikina, T., Suzuki, K., Uematsu, S., Yukawa, K., Kashiwamura, S.-I., Tsutsui, H., Yamamoto, M., Takamatsu, H., Ko-Mitamura, E.P., et al. (2005). Nonredundant roles of Sema4A in the immune system: defective T cell priming and Th1/Th2 regulation in Sema4A-deficient mice. Immunity *22*, 305–316.

Kurup, N., and Jin, Y. (2016). Neural circuit rewiring: insights from DD synapse remodeling. Worm *5*, e1129486.

Lin, K.B.L., Freeman, S.A., Zabetian, S., Brugger, H., Weber, M., Lei, V., Dang-Lawson, M., Tse, K.W.K., Santamaria, R., Batista, F.D., et al. (2008). The Rap GTPases Regulate B Cell Morphology, Immune-Synapse Formation, and Signaling by Particulate B Cell Receptor Ligands. Immunity *28*, 75–87.

Lin, K.B.L., Freeman, S.A., and Gold, M.R. (2010). Rap GTPase-mediated adhesion and migration. Cell Adhes. Migr. *4*, 327–332.

Liu, Z., Fujii, T., Nukazuka, A., Kurokawa, R., Suzuki, M., Fujisawa, H., and Takagi, S. (2005). C. elegans PlexinA PLX-1 mediates a cell contact-dependent stop signal in vulval precursor cells. Dev. Biol. *282*, 138–151.

Luchino, J., Hocine, M., Amoureux, M.-C., Gibert, B., Bernet, A., Royet, A., Treilleux, I., Lécine, P., Borg, J.-P., Mehlen, P., et al. (2013). Semaphorin 3E suppresses tumor cell death triggered by the plexin D1 dependence receptor in metastatic breast cancers. Cancer Cell *24*, 673–685.

Lundquist, E. (2006). Small GTPases. WormBook.

M Bate, A Martinez-Arias (Eds.) The Development of Drosophila Melanogaster. Cold Spring Harb. Press 1363–1491.

Mahmoudi, T., Li, V.S.W., Ng, S.S., Taouatas, N., Vries, R.G.J., Mohammed, S., Heck, A.J., and Clevers, H. (2009). The kinase TNIK is an essential activator of Wnt target genes. EMBO J. *28*, 3329–3340.

Maridonneau-Parini, I., and Gunzburg, J. de (1992). Association of rap1 and rap2 proteins with the specific granules of human neutrophils. Translocation to the plasma membrane during cell activation. J. Biol. Chem. *267*, 6396–6402.

Meyer, M.P., and Smith, S.J. (2006). Evidence from in vivo imaging that synaptogenesis guides the growth and branching of axonal arbors by two distinct mechanisms. J. Neurosci. Off. J. Soc. Neurosci. *26*, 3604–3614.

Mikryukov, A., and Moss, T. (2012). Agonistic and Antagonistic Roles for TNIK and MINK in Non-Canonical and Canonical Wnt Signalling. PLOS ONE *7*, e43330.

Miller, D.M., and Niemeyer, C.J. (1995). Expression of the unc-4 homeoprotein in Caenorhabditis elegans motor neurons specifies presynaptic input. Dev. Camb. Engl. *121*, 2877–2886.

Mitin, N., Rossman, K.L., and Der, C.J. (2005). Signaling Interplay in Ras Superfamily Function. Curr. Biol. *15*, R563–R574.

Mizumoto, K., and Shen, K. (2013a). Two Wnts instruct topographic synaptic innervation in C. elegans. Cell Rep. *5*, 389–396.

Mizumoto, K., and Shen, K. (2013b). Interaxonal interaction defines tiled presynaptic innervation in C. elegans. Neuron *77*, 655–666.

Mombaerts, P., Wang, F., Dulac, C., Chao, S.K., Nemes, A., Mendelsohn, M., Edmondson, J., and Axel, R. (1996). Visualizing an olfactory sensory map. Cell *87*, 675–686.

Mori, K., and Yoshihara, Y. (1995). Molecular recognition and olfactory processing in the mammalian olfactory system. Prog. Neurobiol. *45*, 585–619.

Mori, K., Takahashi, Y.K., Igarashi, K.M., and Yamaguchi, M. (2006). Maps of Odorant Molecular Features in the Mammalian Olfactory Bulb. Physiol. Rev. *86*, 409–433.

Myagmar, B.-E., Umikawa, M., Asato, T., Taira, K., Oshiro, M., Hino, A., Takei, K., Uezato, H., and Kariya, K. (2005). PARG1, a protein-tyrosine phosphatase-associated RhoGAP, as a putative Rap2 effector. Biochem. Biophys. Res. Commun. *329*, 1046–1052.

Myers, K.R., and Casanova, J.E. (2008). Regulation of actin cytoskeleton dynamics by Arf-family GTPases. Trends Cell Biol. *18*, 184–192.

Nakao, F., Fujii, T., Suto, F., Fujisawa, H., and Takagi, S. (1999). An analysis of C.elegans plexin genes. In International C. Elegans Meeting, p.

Nancy, V., Wolthuis, R.M.F., Tand, M.-F. de, Janoueix-Lerosey, I., Bos, J.L., and Gunzburg, J. de (1999). Identification and Characterization of Potential Effector Molecules of the Ras-related GTPase Rap2. J. Biol. Chem. *274*, 8737–8745.

Negishi-Koga, T., Shinohara, M., Komatsu, N., Bito, H., Kodama, T., Friedel, R.H., and Takayanagi, H. (2011). Suppression of bone formation by osteoclastic expression of semaphorin 4D. Nat. Med. *17*, 1473–1480.

Nobes, C.D., and Hall, A. (1995). Rho, Rac, and Cdc42 GTPases regulate the assembly of multimolecular focal complexes associated with actin stress fibers, lamellipodia, and filopodia. Cell *81*, 53–62.

Nonaka, H., Takei, K., Umikawa, M., Oshiro, M., Kuninaka, K., Bayarjargal, M., Asato, T., Yamashiro, Y., Uechi, Y., Endo, S., et al. (2008). MINK is a Rap2 effector for phosphorylation of the postsynaptic scaffold protein TANC1. Biochem. Biophys. Res. Commun. *377*, 573–578.

Nonet, M.L., Staunton, J.E., Kilgard, M.P., Fergestad, T., Hartwieg, E., Horvitz, H.R., Jorgensen, E.M., and Meyer, B.J. (1997). Caenorhabditis elegans rab-3 Mutant Synapses Exhibit Impaired Function and Are Partially Depleted of Vesicles. J. Neurosci. *17*, 8061–8073.

Ohba, Y., Mochizuki, N., Matsuo, K., Yamashita, S., Nakaya, M., Hashimoto, Y., Hamaguchi, M., Kurata, T., Nagashima, K., and Matsuda, M. (2000). Rap2 as a Slowly Responding Molecular Switch in the Rap1 Signaling Cascade. Mol. Cell. Biol. *20*, 6074–6083.

Oinuma, I., Ishikawa, Y., Katoh, H., and Negishi, M. (2004). The Semaphorin 4D Receptor Plexin-B1 Is a GTPase Activating Protein for R-Ras. Science *305*, 862–865.

Pannekoek, W.-J., Linnemann, J.R., Brouwer, P.M., Bos, J.L., and Rehmann, H. (2013). Rap1 and Rap2 Antagonistically Control Endothelial Barrier Resistance. PLOS ONE *8*, e57903.

Park, D.-S., Seo, J.-H., Hong, M., and Choi, S.-C. (2013). Role of the Rap2/TNIK kinase pathway in regulation of LRP6 stability for Wnt signaling. Biochem. Biophys. Res. Commun. *436*, 338–343.

Pascoe, H.G., Wang, Y., and Zhang, X. (2015a). Structural mechanisms of plexin signaling. Prog. Biophys. Mol. Biol. *118*, 161–168.

Pascoe, H.G., Wang, Y., and Zhang, X. (2015b). Structural mechanisms of plexin signaling. Prog. Biophys. Mol. Biol. *118*, 161–168.

Pecho-Vrieseling, E., Sigrist, M., Yoshida, Y., Jessell, T.M., and Arber, S. (2009). Specificity of Sensory-Motor Connections Encoded by Sema3e-PlexinD1 Recognition. Nature *459*, 842–846.

Poinat, P., De Arcangelis, A., Sookhareea, S., Zhu, X., Hedgecock, E.M., Labouesse, M., and Georges-Labouesse, E. (2002). A Conserved Interaction between β1 Integrin/PAT-3 and Nck-Interacting Kinase/MIG-15 that Mediates Commissural Axon Navigation in C. elegans. Curr. Biol. *12*, 622–631.

Ressler, K.J., Sullivan, S.L., and Buck, L.B. (1994). Information coding in the olfactory system: evidence for a stereotyped and highly organized epitope map in the olfactory bulb. Cell *79*, 1245–1255.

Ridley, A.J., and Hall, A. (1992). The small GTP-binding protein rho regulates the assembly of focal adhesions and actin stress fibers in response to growth factors. Cell *70*, 389–399.

Ridley, A.J., Paterson, H.F., Johnston, C.L., Diekmann, D., and Hall, A. (1992). The small GTP-binding protein rac regulates growth factor-induced membrane ruffling. Cell *70*, 401–410.

Rohm, B., Rahim, B., Kleiber, B., Hovatta, I., and Püschel, A.W. (2000). The semaphorin 3A receptor may directly regulate the activity of small GTPases. FEBS Lett. *486*, 68–72.

Schwamborn, J.C., and Püschel, A.W. (2004). The sequential activity of the GTPases Rap1B and Cdc42 determines neuronal polarity. Nat. Neurosci. N. Y. *7*, 923–929.

Shakir, M.A., Gill, J.S., and Lundquist, E.A. (2006). Interactions of UNC-34 Enabled With Rac GTPases and the NIK Kinase MIG-15 in *Caenorhabditis elegans* Axon Pathfinding and Neuronal Migration. Genetics *172*, 893–913.

Shan, G., Kim, K., Li, C., and Walthall, W.W. (2005). Convergent genetic programs regulate similarities and differences between related motor neuron classes in Caenorhabditis elegans. Dev. Biol. *280*, 494–503.

Shang, G., Brautigam, C.A., Chen, R., Lu, D., Torres-Vázquez, J., and Zhang, X. (2017). Structure analyses reveal a regulated oligomerization mechanism of the PlexinD1/GIPC/myosin VI complex. eLife *6*, e27322.

Shaye, D.D., and Greenwald, I. (2011). OrthoList: A Compendium of C. elegans Genes with Human Orthologs. PLOS ONE *6*, e20085.

Shen, K., and Bargmann, C.I. (2003). The immunoglobulin superfamily protein SYG-1 determines the location of specific synapses in C. elegans. Cell *112*, 619–630.

Shitashige, M., Satow, R., Jigami, T., Aoki, K., Honda, K., Shibata, T., Ono, M., Hirohashi, S., and Yamada, T. (2010). Traf2- and Nck-Interacting Kinase Is Essential for Wnt Signaling and Colorectal Cancer Growth. Cancer Res. *70*, 5024–5033.

Shkoda, A., Town, J.A., Griese, J., Romio, M., Sarioglu, H., Knöfel, T., Giehler, F., and Kieser, A. (2012). The Germinal Center Kinase TNIK Is Required for Canonical NF-κB and JNK Signaling in B-Cells by the EBV Oncoprotein LMP1 and the CD40 Receptor. PLOS Biol. *10*, e1001376.

Stewart, W.B., Kauer, J.S., and Shepherd, G.M. (1979). Functional organization of rat olfactory bulb analysed by the 2-deoxyglucose method. J. Comp. Neurol. *185*, 715–734.

Stinchcomb, D.T., Shaw, J.E., Carr, S.H., and Hirsh, D. (1985). Extrachromosomal DNA transformation of Caenorhabditis elegans. Mol. Cell. Biol. *5*, 3484–3496.

Sun, H.Q., Yamamoto, M., Mejillano, M., and Yin, H.L. (1999). Gelsolin, a multifunctional actin regulatory protein. J. Biol. Chem. *274*, 33179–33182.

Tada, M., Gengyo-Ando, K., Kobayashi, T., Fukuyama, M., Mitani, S., Kontani, K., and Katada, T. (2012). Neuronally expressed Ras-family GTPase Di-Ras modulates synaptic activity in Caenorhabditis elegans. Genes Cells *17*, 778–789.

Taira, K., Umikawa, M., Takei, K., Myagmar, B.-E., Shinzato, M., Machida, N., Uezato, H., Nonaka, S., and Kariya, K. (2004). The Traf2- and Nck-interacting Kinase as a Putative Effector of Rap2 to Regulate Actin Cytoskeleton. J. Biol. Chem. *279*, 49488–49496.

Takai, Y., Kaibuchi, K., Kikuchi, A., and Kawata, M. (1992). Small GTP-Binding Proteins. Int. Rev. Cytol. *133*, 187–230.

Takai, Y., Sasaki, T., and Matozaki, T. (2001). Small GTP-binding proteins. Physiol. Rev. *81*, 153–208.

Tamagnone, L., Artigiani, S., Chen, H., He, Z., Ming, G., Song, H., Chedotal, A., Winberg, M.L., Goodman, C.S., Poo, M., et al. (1999). Plexins Are a Large Family of Receptors for Transmembrane, Secreted, and GPI-Anchored Semaphorins in Vertebrates. Cell *99*, 71–80.

Tapon, N., and Hall, A. (1997). Rho, Rac and Cdc42 GTPases regulate the organization of the actin cytoskeleton. Curr. Opin. Cell Biol. *9*, 86–92.

Timofeev, K., Joly, W., Hadjieconomou, D., and Salecker, I. (2012). Localized Netrins Act as Positional Cues to Control Layer-Specific Targeting of Photoreceptor Axons in Drosophila. Neuron *75*, 80–93.

Tomas, A., Yermen, B., Min, L., Pessin, J.E., and Halban, P.A. (2006). Regulation of pancreatic β-cell insulin secretion by actin cytoskeleton remodelling: role of gelsolin and cooperation with the MAPK signalling pathway. J. Cell Sci. *119*, 2156–2167.

Torti, M., Bertoni, A., Canobbio, I., Sinigaglia, F., Lapetina, E.G., and Balduini, C. (1999). Interaction of the low-molecular-weight GTP-binding protein rap2 with the platelet cytoskeleton is mediated by direct binding to the actin filaments. J. Cell. Biochem. *75*, 675–685.

Toyofuku, T., and Kikutani, H. (2007). Semaphorin Signaling During Cardiac Development. In Semaphorins: Receptor and Intracellular Signaling Mechanisms, R.J. Pasterkamp, ed. (Springer New York), pp. 109–117.

Toyofuku, T., Yoshida, J., Sugimoto, T., Yamamoto, M., Makino, N., Takamatsu, H., Takegahara, N., Suto, F., Hori, M., Fujisawa, H., et al. (2008). Repulsive and attractive semaphorins cooperate to direct the navigation of cardiac neural crest cells. Dev. Biol. *321*, 251–262.

Trujillo-Cenóz, O. (1965). Some aspects of the structural organization of the intermediate retina of dipterans. J. Ultrastruct. Res. *13*, 1–33.

Trujillo-Cenoz and Melamed (1966). Electron microscope observations on the peripheral and intermediate retinas of dipterans. Pergamon Press 339–361.

Vassar, R., Chao, S.K., Sitcheran, R., Nuñez, J.M., Vosshall, L.B., and Axel, R. (1994). Topographic organization of sensory projections to the olfactory bulb. Cell *79*, 981–991.

Vigier, P (1909). Mécanisme de la synthese des impressions lumineuses recueilles par les yeux composés des Dipteres. CR Acad Sci 1221–1223.

Vigil, D., Cherfils, J., Rossman, K.L., and Der, C.J. (2010). Ras superfamily GEFs and GAPs: validated and tractable targets for cancer therapy? Nat. Rev. Cancer *10*, 842–857.

Wang, Q., Charych, E., Pulito, V., Lee, J., Graziane, N., Crozier, R., Revilla-Sanchez, R., Kelly, M., Dunlop, A., Murdoch, H., et al. (2011). The psychiatric disease risk factors DISC1 and TNIK interact to regulate synapse composition and function. Mol. Psychiatry *16*, 1006–1023.

Wang, Y., Pascoe, H.G., Brautigam, C.A., He, H., and Zhang, X. (2013). Structural basis for activation and non-canonical catalysis of the Rap GTPase activating protein domain of plexin. eLife *2*, e01279.

Weston, C.R., and Davis, R.J. (2007). The JNK signal transduction pathway. Curr. Opin. Cell Biol. *19*, 142–149.

White, J.G., Southgate, E., Thomson, J.N., and Brenner, S. (1976). The Structure of the Ventral Nerve Cord of Caenorhabditis elegans. Philos. Trans. R. Soc. Lond. B Biol. Sci. *275*, 327–348.

White, J.G., Albertson, D.G., and Anness, M.A. (1978). Connectivity changes in a class of motoneurone during the development of a nematode. Nature *271*, 764–766.

Winberg, M.L., Noordermeer, J.N., Tamagnone, L., Comoglio, P.M., Spriggs, M.K., Tessier-Lavigne, M., and Goodman, C.S. (1998). Plexin A Is a Neuronal Semaphorin Receptor that Controls Axon Guidance. Cell *95*, 903–916.

Yaman, E., Gasper, R., Koerner, C., Wittinghofer, A., and Tazebay, U.H. (2009). RasGEF1A and RasGEF1B are guanine nucleotide exchange factors that discriminate between Rap GTP-binding proteins and mediate Rap2-specific nucleotide exchange. FEBS J. *276*, 4607–4616.

Yang, D.-S., Roh, S., and Jeong, S. (2016). The axon guidance function of Rap1 small GTPase is independent of PlexA RasGAP activity in Drosophila. Dev. Biol. *418*, 258–267.

Yang, Y., Lee, W.S., Tang, X., and Wadsworth, W.G. (2014). Extracellular matrix regulates UNC-6 (netrin) axon guidance by controlling the direction of intracellular UNC-40 (DCC) outgrowth activity. PloS One *9*, e97258.

Yin, H.L., and Stossel, T.P. (1979). Control of cytoplasmic actin gel–sol transformation by gelsolin, a calcium-dependent regulatory protein. Nature *281*, 583–586.

Yoo, S.K., Pascoe, H.G., Pereira, T., Kondo, S., Jacinto, A., Zhang, X., and Hariharan, I.K. (2016). Plexins function in epithelial repair in both Drosophila and zebrafish. Nat. Commun. *7*, 12282.

Yu, D.-H., Zhang, X., Wang, H., Zhang, L., Chen, H., Hu, M., Dong, Z., Zhu, G., Qian, Z., Fan, J., et al. (2014). The essential role of TNIK gene amplification in gastric cancer growth. Oncogenesis *3*, e89.

Zand, T.P., Reiner, D.J., and Der, C.J. (2011). Ras Effector Switching Promotes Divergent Cell Fates in C. elegans Vulval Patterning. Dev. Cell *20*, 84–96.

Zecevic, N., and Rakic, P. (1991). Synaptogenesis in monkey somatosensory cortex. Cereb. Cortex N. Y. N 1991 *1*, 510–523.

Zhu, Y., Pak, D., Qin, Y., McCormack, S.G., Kim, M.J., Baumgart, J.P., Velamoor, V., Auberson, Y.P., Osten, P., van Aelst, L., et al. (2005a). Rap2-JNK Removes Synaptic AMPA Receptors during Depotentiation. Neuron *46*, 905–916.

Zhu, Y., Pak, D., Qin, Y., McCormack, S.G., Kim, M.J., Baumgart, J.P., Velamoor, V., Auberson, Y.P., Osten, P., van Aelst, L., et al. (2005b). Rap2-JNK Removes Synaptic AMPA Receptors during Depotentiation. Neuron *46*, 905–916.